Epicyclic oscillations of test particles near marginally stable circular orbits around charged Kiselev black holes

Dmitriy Ovchinnikov,[1,*] Muhammad Umar Farooq,[2,†] Ibrar Hussain,[3,‡] Ahmadjon Abdujabbarov,[4,5,6,7,§] Bobomurat Ahmedov,[5,6,7,¶] and Zdeněk Stuchlík[1,**]

[1]*Research Centre for Theoretical Physics and Astrophysics, Institute of Physics, Silesian University in Opava, Bezrucovo namesti 13, CZ-746 01 Opava, Czech Republic*
[2]*Department of Basic Sciences and Humanities, College of Electrical and Mechanical Engineering, National University of Sciences and Technology, H-12, Islamabad 44000, Pakistan*
[3]*School of Electrical Engineering and Computer Science, National University of Sciences and Technology, H-12 Campus, Islamabad 44000, Pakistan*
[4]*Shanghai Astronomical Observatory, 80 Nandan Road, Shanghai 200030, China*
[5]*Ulugh Beg Astronomical Institute, Astronomy Street 33, Tashkent 100052, Uzbekistan*
[6]*National University of Uzbekistan, Tashkent 100174, Uzbekistan*
[7]*Tashkent Institute of Irrigation and Agricultural Mechanization Engineers, Kori Niyoziy, 39, Tashkent 100000, Uzbekistan*

(Received 4 August 2020; accepted 4 August 2021; published 15 September 2021)

The marginally stable circular orbits (MSCOs) of test particles in the spacetime exterior to a charged Kiselev black hole are investigated for three characteristic values of the equation of state parameter ω_q, namely (i) $\omega_q = -1/3$, (ii) $\omega_q = -1$, and (iii) $\omega_q = -2/3$, and for different values of the normalization factor α and electric charge Q of the black hole. It is found that the presence of the quintessence field shifts outward the innermost stable circular orbits (ISCOs) around the Kiselev black hole, having the same charge parameter Q, as compared to the ISCOs around a Riessner-Nordstrom black hole, while the effect of the quintessence field on the outermost stable circular orbits (OSCOs) is just opposite to that on the ISCOs. Further, the radii of the photon circular orbits are also calculated for different ranges of the parameters α and Q. It is observed that the photon orbits are also shifted outward as the value of α increases. The radial and latitudinal epicyclic motion of test particles, which can be related to the quasiperiodic oscillations of test particles slightly above the MSCOs in the vicinity of the charged Kiselev black hole, is analyzed for the three different values of ω_q. It is seen that the azimuthal and latitudinal frequencies coincide, and the radial epicyclic frequency is different in dependence on the spacetime parameters. In the case of $\omega_q = -1/3$, the azimuthal and latitudinal frequencies depend on the radial position r of the particle, the charge Q, and the mass M of the black hole, and do not depend on the factor α. However, for $\omega_q = -2/3$ and $\omega_q = -1$, these two frequencies, along with the black hole parameters—i.e., M and Q and the radial position r—also depend on the factor α. The radial epicyclic frequency for all the values of ω_q depends on M, Q, r, and also on the normalization factor α. We also compare the epicyclic frequencies with that for an uncharged black hole. With the increase of electric charge, the ISCO becomes closer to the central object, and one can observe epicyclic frequencies closer to the central object, which makes the epicyclic frequencies larger. The ISCO gets larger as α increases, and thus the epicyclic frequencies can be observed away from the central object and would be smaller as compared to the case of a pure Riessner-Nordstrom black hole without quintessence. As the effect of the parameters Q and α on the OSCOs is just opposite to that on the ISCOs, the epicyclic frequencies near the OSCOs behave the other way around.

DOI: 10.1103/PhysRevD.104.063027

I. INTRODUCTION

According to the predictions of general relativity (GR), astrophysical black holes in the mass range 3–30 $M_\odot$ are formed as a result of the gravitational collapse of the end product of the evolution of massive stars in the range 10–200 $M_\odot$. From the astrophysical point of view, the accretion disks orbiting black holes are the most relevant

*dmitriy.ovchinnikov@fpf.slu.cz
†m_ufarooq@yahoo.com
‡ibrar.hussain@seecs.nust.edu.pk
§ahmadjon@astrin.uz
¶ahmedov@astrin.uz
**zdenek.stuchlik@physics.slu.cz

objects, being governed by the circular geodesics of the black hole's close environment. Therefore, any study of the dynamics of particles in the vicinity of black holes may be helpful in comprehending the surrounding gravitational field in the strong gravity regime. A vast literature exists on this topic—e.g., Refs. [1–29]. However, astronomical and astrophysical large-scale observations of the Universe [30] indicate the crucial role of dark energy that can be treated as a vacuum energy (cosmological constant) or quintessential field [31]. Dark energy can have a significant role in the astrophysical phenomena related to supermassive black holes in galactic nuclei. In the case of the cosmological constant, such effects were treated in a series of works (see Refs. [32–44]). Quintessential black holes were first introduced by Kiselev [45], and their rotational form was discussed in Refs. [42,46]. The basic properties of such black holes were investigated in Refs. [47–49]. A fundamental comment on the Kiselev black hole solution has been presented in Ref. [50]. Here, we concentrate on the exploration of the static and charged version of the Kiselev black hole, to investigate the positions of the innermost stable circular orbits (ISCOs) and outermost stable circular orbits (OSCOs), and how they are affected by the black hole parameters along with the quintessence field. In GR, the radii of circular orbits for the particles in the vicinity of black holes have lower bounds, and these orbits are the ISCOs, while circular orbits at the upper bound on their radii are the OSCOs. The ISCOs and OSCOs form a boundary between the two regions—i.e., the stable region and the unstable region. In the literature, this boundary is termed as the marginally stable circular orbits (MSCOs). If in some spacetime geometry there are only two MSCOs, then the smaller one is known as the ISCO and the larger one is called the OSCO. If there are more than two MSCOs in a spacetime geometry, then the smallest is the ISCO and the largest one is the OSCO.

To explain the nature of dark energy, among the others, there is a model that examines the possibility of the existence of the quintessence scalar field (see, e.g., Ref. [51]). The equation of negative state parameter (ratio of the pressure and density) defines the quintessence scalar field [52]. The black hole solution with quintessences, of the Einstein field equations [45], has been studied by different authors from different points of view (see Refs. [53–59]). The charged Kiselev black hole solution reduces to the Reissner-Nordström black hole solution of the field equations in the limiting case when the quintessence term tends to zero. If the charge term also tends to zero, then this black hole solution reduces to the Schwarzschild black hole solution. The motion of photons in the vicinity of the Kiselev black hole has been studied by Sharmanthie Fernando for some specific values of the equation of state parameter $\omega_q = -2/3$ and of the normalization factor $\alpha = 0.1, 0.01, 0.005$ [11] (α is given in the metric coefficient of the line element of the charged Kiselev black hole in Sec. III). The motion of massive particles around a Kiselev black hole has been analyzed by Rashmi *et al.* for $\omega_q = -1, -2/3, -1/3$ and $\alpha = 0.1, 0.08, 0.05, 0.005$ [25]. For a unit mass black hole with $\omega_q = -1/3, -2/3$ and $\alpha = 0.1$, they have shown that the ISCOs are bigger than those of the Schwarzschild black hole. The existence of such MSCOs for Kottler black hole spacetimes was given using Sturm's theorem in Ref. [32], and later repeated in Ref. [26]. Recently, the MSCOs of the Kiselev back hole for three different values of the equation of state parameter $\omega_q = -1, -2/3, -1/3$ have been investigated, and upper and lower bounds were obtained on the value of the normalization factor α for the existence of MSCOs [58]. In the present study, we are interested in the investigation of the MSCOs in the spacetime geometry of a charged Kiselev black hole. In particular, we are keen to look at the effects of the quintessence on the MSCOs in the charged Kiselev black hole spacetime.

A very interesting phenomenon of the particle dynamics in black hole spacetimes is related to the quasiperiodic oscillations (QPOs) detected in the x-ray radiation of microquasars. Microquasars are binary systems of a black hole surrounded by an accretion disk consisting of matter flowing from a companion star. Friction in the orbiting accretion disk in the vicinity of the ISCO is so strong that the matter of the accretion disk also starts to emit x rays. The friction between layers of the disk causes a decrease of the energy and angular momentum of nearly freely orbiting matter in accordance with the energy and angular momentum radial profiles of geodesic circular motion. The QPOs are very important from the astrophysical point of view, because they are considered to be one of the most efficient tests of strong gravity models and a useful tool for the precise measurement of black hole parameters. In this regard, the QPOs from accreting black holes have been studied by many scientists, and some of the results can be found in literature [60–63]. To explain the nature of the QPOs, various theoretical models, including disk-seismic models, hot-spot models, warped disk models, and resonance models have been proposed [64].

It is important that for both Keplerian thin accretion disks governed by energetics of stable circular geodetics of the spacetime [65,66] and slightly extended tori that are in equilibrium due to pressure gradients [67], the frequencies of their oscillations are governed by the frequencies of the epicyclic oscillatory motion around circular geodesics, thus giving the so-called geodesic (epicyclic) models of the QPOs obtained in microquasars or around supermassive black holes in active galactic nuclei. Direct generalization of the geodesic models can be obtained if electromagnetic interaction of a slightly charged hot spot with a large-scale magnetic field around a black hole is included in the calculation of the frequencies of the epicyclic oscillations [68–71]. The role of the synchrotron radiation representing

a special kind of friction acting on moving charged particles has been discussed in the literature [72].

QPOs observed in the x-ray spectra are widely believed to be related to oscillations in regions of accretion disks close to the ISCO [73]. Here we analyze the crucial quantities for oscillation models based on the geodetic epicyclic motion—namely, the orbital, radial, and latitudinal epicyclic frequencies of test particles close to the stable circular orbits in the vicinity of the charged Kiselev black hole, for the three different values of ω_q.

The spacetime geometry of the charged Kiselev black hole is discussed in Sec. II. The conditions for the existence of MSCOs for a general spherically symmetric static spacetime are given in Sec. III. Then, in Sec. III, we also investigate MSCOs in the vicinity of the charged Kiselev back hole for the three different values of the equation-of-state parameter ω_q, where we find that the radii of the ISCOs and OSCOs vary for different values of the charge Q and quintessence parameter α. Interestingly, we have obtained bounds on the values of Q and α for the existence of the charged Kiselev black hole. In Sec. IV, we study the fundamental frequencies of test particles in the spacetime field of the charged Kiselev black hole for the three cases of ω_q and have observed how these fundamental frequencies are affected by Q and α. A summary of our results is presented in Sec. V. In the present study, we use geometric units ($G = c = 1$) and $\hbar = 1$, where G is the Newtonian gravitational constant, c is the speed of light in vacuum, and $\hbar$ is the reduced Planck constant. The metric signature is taken as $(-,+,+,+)$, and the greek (latin) indices run from 0 to 3 (1 to 3).

II. SPACETIME GEOMETRY OF THE CHARGED KISELEV BLACK HOLE

General spherically symmetric static spacetime is represented by the line element

$$\mathrm{d}s^2 = -N(r)\mathrm{d}t^2 + \frac{1}{N(r)}\mathrm{d}r^2 + r^2(\mathrm{d}\theta^2 + \sin^2\theta\mathrm{d}\phi^2), \tag{1}$$

where the metric coefficient $N(r)$ is called the lapse function. For the charged Kiselev black hole, which is extensively studied in the literature from different points of view (for example, Refs. [47,53,74–87]), the function $N(r)$ takes the following form [45]:

$$N(r) = 1 - \frac{2M}{r} - \frac{\alpha}{r^{3\omega_q+1}} + \frac{Q^2}{r^2}. \tag{2}$$

Using the standard procedure, the electric charge Q and the ADM mass M of the black hole can be calculated as [88]

$$Q = \frac{1}{4\pi}\int \nabla_\alpha A_{t*} dS^\alpha, \tag{3}$$

$$M = \frac{1}{4\pi}\lim_{S^\alpha \to i^0}\int g^{\mu\nu}(\partial_\beta g_{\mu\alpha} - \partial_\mu g_{\alpha\beta})_* dS^\alpha, \tag{4}$$

where ${}_*dS^\alpha$ is the dual element of the hypersurface $dS^{\alpha\beta\gamma}$, i^0 is the spacelike infinity when the normalization factor α (which is related to the cosmological constant in the case where $\omega_q = -1$) is equal to zero, and ∂_α stands for the partial derivative with respect to coordinate x^α. In the case of a nonzero normalization factor α for $\omega_q < -1/3$, spacetime is not flat at infinity, and we cannot give the interpretation of the parameters M and Q as the total mass and electric charge of the central black hole. Although there is no generally accepted interpretation of these quantities in asymptotically de Sitter spacetime, there are some different points of view on this problem—see, for example, Ref. [89], where the author gives a definition of the parameter M as the Noether charge. The interpretation of the parameters M and Q as the total mass and electric charge of the central black hole is possible only in the asymptotically flat spacetime case when the parameter α vanishes.

The parameter ω_q is responsible for the equation of state of the surrounding matter. Depending on the values of the parameter ω_q, the corresponding equation of state may represent different matter surrounding the compact object. Particularly, $\omega_q = 0$ corresponds to an ideal gas, while $\omega_q = 1/3$ represents the ultrarelativistic particles, including neutrinos. Negative values of ω_q represent some exotic matter used in some models of dark matter and dark energy. On the other hand, hypothetical so-called phantom energy corresponds to the value $\omega_q < -1$, which can cause a big rip. Current cosmological observational data cannot distinguish whether space is fulfilled with phantom ($\omega_q < -1$) or nonphantom ($\omega_q \geq -1$) matter [90]. For the quintessence, it takes values in the interval $-1 < \omega_q < -1/3$ in order to have the observed accelerated expansion of the cosmos [45]. The extreme case of $\omega_q = -1$ corresponds to the cosmological constant, while the other extreme value of the parameter—i.e., $\omega_q = -1/3$—corresponds to the frustrated network of strings, for which the Universe remains static and which is discussed in great detail in the literature [91–93]. The case of $\omega_q = -1/3$ has been considered by different authors in different scenarios (see, for example, Refs. [25,58,85]). In the original paper [45], it is shown that parameter ω_q is related to the equation of state for the quintessence matter with isotropic negative pressure p_q by the relation

$$p_q = \omega_q \rho_q, \tag{5}$$

where ρ_q is the energy density given by

$$\rho_q = \frac{3}{8\pi}\frac{\alpha\omega_q}{r^{3(1+\omega_q)}}. \tag{6}$$

In this work, we are interested only in studying the charged Kiselev black hole (the spacetime where three distinct horizons exist: the inner horizon r_{ih}, the event horizon r_{eh}, and the cosmological horizon r_{ch}, and where $r_{ih} < r_{eh} < r_{ch}$). We should mention that we also consider the limiting case $\omega_q = -1/3$; for this value, spacetime is flat at infinity and there is no cosmological horizon. We also constrain our calculation to the region $r_{eh} < r < r_{ch}$, because only in this region is the trajectory of the particles relevant. The lapse function [Eq. (2)] in this region takes positive values: $N(r)\rangle 0$ [$N(r) < 0$ for $0 < r < r_{ih}$ and $r > r_{ch}$]. The range where values of the parameter α can change depends on the chosen parameters ω_q and Q (for each value of the parameter ω_q, limits are discussed later in the text) and is similar to that for an uncharged Kiselev black hole (where α depends on ω only), as is shown in Ref. [25]. In the case where $\alpha = 0$, the black hole reduces to the Reissner-Nordström black hole, and if $Q = 0$ also, it reduces to the Schwarzschild black hole. A detailed discussion on the horizon structure of the Kiselev black hole is presented in Refs. [57,77].

III. EQUATIONS OF MOTION AND CONDITIONS FOR THE EXISTENCE OF MSCOs

Equations of motion can be found by the Hamilton-Jacobi method. The Hamilton-Jacobi equation in the general case for the Hamiltonian function, defined as

$$H = \frac{1}{2} g^{\mu\nu} p_\mu p_\nu, \tag{7}$$

can be written as

$$-\frac{\partial S}{\partial \tau} = \frac{1}{2} g^{\mu\nu} \frac{\partial S}{\partial x^\mu} \frac{\partial S}{\partial x^\nu}, \tag{8}$$

where τ is the proper time in the case of massive particles (in the case of massless particles, we should exchange τ with another affine parameter λ), the function S is the action for a particle moving along a geodesic, and p_μ is the components of the four-momentum written as partial derivatives of the action S with respect to coordinates x^μ:

$$\frac{\partial S}{\partial x^\mu} = p_\mu. \tag{9}$$

For the spacetime described by the metric in Eq. (1) with the metric function $N(r)$ given by Eq. (2), the Hamilton-Jacobi equation can be written as

$$-\frac{\partial S}{\partial \tau} = -\frac{1}{2N(r)} \left(\frac{\partial S}{\partial t}\right)^2 + \frac{1}{2} N(r) \left(\frac{\partial S}{\partial r}\right)^2 + \frac{1}{2r^2} \left(\frac{\partial S}{\partial \theta}\right)^2 + \frac{1}{2r^2 \sin^2\theta} \left(\frac{\partial S}{\partial \phi}\right)^2. \tag{10}$$

Since we are considering the stationary spherically symmetric spacetime, we can try to find the solution to the Hamilton-Jacobi equation in separable form:

$$S(\tau, t, r, \theta, \phi) = S_\tau(\tau) + S_t(t) + S_r(r) + S_\theta(\theta) + S_\phi(\phi). \tag{11}$$

The subscripts of the functions $S_\tau(\tau)$, $S_t(t)$, $S_r(r)$, $S_\theta(\theta)$, and $S_\phi(\phi)$ should not be considered as indices of the components of some vector.

Using the normalization condition for the massive particle

$$p^\mu p_\mu = -m^2, \tag{12}$$

where m is the rest mass of the test particle ($m = 0$ for photons), and comparing it with the Hamilton-Jacobi equations, we show that

$$\frac{\partial S}{\partial \tau} = \frac{\partial S_\tau(\tau)}{\partial \tau} = \frac{1}{2} m^2. \tag{13}$$

Since the Hamiltonian does not depend explicitly on the coordinates t and ϕ, from the Hamilton equations

$$\frac{\mathrm{d}p_\mu}{\mathrm{d}\tau} = -\frac{\partial H}{\partial x^\mu}, \qquad \frac{\mathrm{d}x^\mu}{\mathrm{d}\tau} = \frac{\partial H}{\partial p_\mu}, \tag{14}$$

we write that the components p_t and p_ϕ of the four-momentum are the constants of motion $p_t = -E$ and $p_\phi = L$. It is possible to show that these constants of motion are related to the energy and azimuthal components of the angular momentum of the particle.

According to the Noether theorem, the conservation laws correspond to the isometries of a spacetime. For a test particle with a constant rest mass m and momentum p^μ moving along a geodesic, the geodesic equation can be written as

$$\frac{Dp^\mu}{d\tau} = p^\mu_{;\nu} U^\nu = m U^\mu_{;\nu} U^\nu = 0. \tag{15}$$

If spacetime symmetries allow the existence of a Killing vector ξ^μ satisfying

$$\xi_{\mu;\nu} + \xi_{\nu;\mu} = 0, \tag{16}$$

then the scalar quantity $p_{(\xi)} = p_\mu \xi^\mu$ is conserved along the geodesic trajectory due to Eqs. (15) and (16):

$$dp_{(\xi)}/d\tau = D(p^\mu \xi_\mu) d\tau = p^\mu \xi_{\mu;\nu} U^\nu = m U^\mu \xi_{\mu;\nu} U^\nu = 0. \tag{17}$$

If the Killing vector ξ^μ is timelike, then the scalar quantity $p_{(\xi)}$ can be interpreted as the conserved energy of the

particle. There is always a coordinate system where the curves to which ξ^μ are tangent are coordinate lines along which only the time coordinate $x^0 = t$ changes. It is easy to choose the t coordinate so that in this new coordinate system, the Killing vector is $\xi^\mu = (1, 0, 0, 0)$, and the Killing equation (16) becomes $g_{\mu\nu,t} = 0$, which corresponds to our concept of stationarity. From the statement that there is a timelike Killing vector, it follows that there exists such a coordinate system in which the metric tensor is time-independent. The existence of a spacelike Killing vector in the spacetime is responsible for the conservation of angular momentum of a particle along the geodesic.

Using again the relation which connects components of the four-momentum with derivations of the action S with respect to coordinates, we obtain expressions for the functions $S_t(t)$ and $S_\phi(\phi)$ as follows:

$$\frac{\partial S}{\partial t} = \frac{\partial S_t(t)}{\partial t} = -E, \tag{18}$$

$$\frac{\partial S}{\partial \phi} = \frac{\partial S_\phi(\phi)}{\partial \phi} = L. \tag{19}$$

Using the obtained separable function for the action S, with the functions $S_t(t)$ and $S_\phi(\phi)$, expressed by the constants of motion E and L, the Hamilton-Jacobi equation can be written as

$$\frac{r^2}{N(r)}E^2 - N(r)r^2\left(\frac{\partial S_r}{\partial r}\right)^2 - m^2r^2 = \left(\frac{\partial S_\theta}{\partial \theta}\right)^2 + \frac{L^2}{\sin^2\theta} = C = \text{constant}. \tag{20}$$

Since the left- and right-hand sides of the obtained expression are differential equations which depend on either r or θ, these two equations should be equal to the same constant C, which is the separation constant. For convenience, we introduce the constant K, which is related to the separation constant C by the equation $L^2 + K = C$, and $K = 0$ for a particle moving in the equatorial plane.

From the Hamilton-Jacobi equation, the covariant components of the four-momentum for massive particles can be written as

$$p_t = -E, \tag{21}$$

$$p_r = \pm\sqrt{\frac{1}{N(r)}\left(\frac{E^2}{N(r)} - m^2 + \frac{L^2 + K}{r^2}\right)}, \tag{22}$$

$$p_\theta = \pm\sqrt{K - L^2\cot^2\theta}, \tag{23}$$

$$p_\phi = L. \tag{24}$$

The corresponding contravariant components of the four-momentum are defined as

$$p^t = \frac{E}{N(r)}, \tag{25}$$

$$p^r = \pm\sqrt{E^2 - N(r)\left(m^2 + \frac{L^2 + K}{r^2}\right)}, \tag{26}$$

$$p^\theta = \pm\frac{1}{r^2}\sqrt{K - L^2\cot^2\theta}, \tag{27}$$

$$p^\phi = \frac{L}{r^2\sin^2\theta}. \tag{28}$$

For further calculations, we introduce the specific angular momentum $L \to L/m$ and specific energy $E \to E/m$. It is equivalent to take $m = 1$ in the equations of motion for a massive particle, and using the relation between four-momentum and four-velocity

$$p^\mu = mU^\mu, \tag{29}$$

the equations of motion can be written in the following way:

$$\frac{dt}{d\tau} = \frac{E}{N(r)}, \tag{30}$$

$$\frac{dr}{d\tau} = \pm\sqrt{E^2 - N(r)\left(1 + \frac{L^2 + K}{r^2}\right)}, \tag{31}$$

$$\frac{d\theta}{d\tau} = \pm\frac{1}{r^2}\sqrt{K - L^2\cot^2\theta}, \tag{32}$$

$$\frac{d\phi}{d\tau} = \frac{L}{r^2\sin^2\theta}. \tag{33}$$

Because of the spherical symmetry of the spacetime, any of the central planes can be considered as the equatorial one; for the chosen coordinate system, we fixed the equatorial plane to be at $\theta = \pi/2$.

In the equatorial plane, the equation of motion for the radial coordinate of the massive particle is given by

$$\frac{dr}{d\tau} = \pm\sqrt{E^2 - V_{\text{eff}}(r)}. \tag{34}$$

For studying the motion of particles in the equatorial plane, it is useful to introduce the special function $V_{\text{eff}}(r)$,

$$V_{\text{eff}}(r) = N(r)\left(1 + \frac{L^2}{r^2}\right), \tag{35}$$

by analogy with the function of "effective potential" used for studying particle orbits in asymptotically flat spacetimes.

In the case of massless particles (photons), using Hamilton-Jacobi equations, applying the appropriate normalization condition $p^\mu p_\mu = 0$, and exchanging proper time τ with affine parameter λ, components of the four-momentum can be obtained by the same procedure that was used for massive particles. The radial component of the four-momentum for photons reads as

$$\tilde{p}^r = \pm\sqrt{\tilde{E}^2 - \tilde{V}_{\text{eff}}(r)}, \tag{36}$$

where the function $\tilde{V}_{\text{eff}}(r)$ is equal to

$$\tilde{V}_{\text{eff}}(r) = N(r)\left(\frac{\tilde{L}^2}{r^2}\right). \tag{37}$$

The spacetime under our consideration is asymptotically de Sitter for $\omega_q = -1$ when $\alpha > 0$. In the case of $\omega_q = -2/3$ when $\alpha > 0$, the spacetime under discussion has a cosmological horizon, and particles moving in such spacetime experience a repulsive force acting on them like in the Reisner–Nordstrom–de Sitter spacetime. However, the lapse function does not reduce to that of the Reisner–Nordstrom–de Sitter spacetime in this case. For $\omega_q = -2/3$ and $\omega_q = -1$ when $\alpha > 0$, there is a radius where gravitational attraction is balanced by the repulsive constant α [32]. This position in a spacetime is called the static radius (not to be confused with static orbit in rotating spacetime [94]). The static radius plays a crucial role in the analysis of de Sitter spacetimes, where there is no stable circular orbit with a radius higher than this static radius. In the case of $\omega_q = -1/3$ when $\alpha > 0$, there is no cosmological horizon or static radius.

From the Hamilton equations (14), we can find the radial component of the four-momentum, and then using Eq. (29), we can obtain the equation for the radial component of a particle's four-acceleration:

$$\frac{\mathrm{d}U^r}{\mathrm{d}\lambda} = -\frac{N'(r)}{2N(r)}E^2 + \frac{3N'(r)}{2N(r)}(p^r)^2 + \frac{N(r)}{r^3}L^2, \tag{38}$$

where the prime denotes a derivative with respect to the radial coordinate r. It is expected that for a particle on the static radius in the equatorial plane, the radial component of the four-velocity is equal to zero, $U^r = 0$; the radial four-acceleration is equal to zero, $dU^r/d\lambda = 0$; and at the same time specific angular momentum is also equal to zero, $L = 0$. Applying this condition to Eq. (38), we obtain an equation for the static radius r_{stat} as

$$N'(r) = 0. \tag{39}$$

Further, it is shown that in the case $\omega_q = -2/3$ and $\omega_q = -1$, OSCOs are located inside the static radius (see also Ref. [95]).

For particles moving along a circular orbit, the conditions

$$E^2 = V_{\text{eff}}(r), \qquad V'_{\text{eff}}(r) = 0 \tag{40}$$

should be satisfied. For a particle on a MSCO, the condition

$$V''_{\text{eff}}(r) = 0 \tag{41}$$

should also be satisfied.

From these conditions for massive particles, we get the equation for the radii of MSCOs $r = r_{\text{MSCO}}$ as

$$0 = \frac{4r(N'(r))^2 - 6N(r)N'(r) - 2rN(r)N''(r)}{(2N(r) - rN'(r))(4rN'(r) - r^2N''(r) - 6N(r))}. \tag{42}$$

Using the conditions given by Eq. (40), one can obtain the expressions for the energy and the angular momentum of a test particle in a circular orbit as

$$E^2 = \frac{2N(r)^2}{2N(r) - rN'(r)}, \tag{43}$$

$$L^2 = \frac{r^3N'(r)}{2N(r) - rN'(r)}. \tag{44}$$

In the following subsections, we study the MSCOs for the charged Kiselev black hole by taking into account the conditions for their existence, given by Eqs. (40) and (41) for the three different values of ω_q—namely, $\omega_q = -1/3$, $\omega_q = -1$, and $\omega_q = -2/3$—in the lapse function $N(r)$ given by Eq. (2).

A. MSCOs for the charged Kiselev black hole with $\omega_q = -1/3$

In this section, we study the particle motion when the parameter $\omega_q = -1/3$. (The special character of this specific version of the black hole solution is treated in detail in Ref. [96].) In this case, the lapse function $N(r)$ takes the following form:

$$N(r) = -\alpha + \frac{Q^2}{r^2} - \frac{2M}{r} + 1. \tag{45}$$

Like the Reissner-Nordström black hole, for the charged Kiselev black hole there is a maximum magnitude of the charge Q for which the event horizon disappears and the spacetime becomes one with a naked singularity. The maximal magnitude of the charge parameter is related with the parameter α by the condition

$$|Q| \leq \frac{M}{\sqrt{(1-\alpha)}}. \tag{46}$$

The maximum magnitude of the charge Q for the charged Kiselev black hole is not equal to M, but depends on the value of the parameter α, and tends to infinity when α goes to 1. In Fig. 1, it is shown how the maximal magnitude of the positive charge $|Q|_{\max} = M/\sqrt{1-\alpha}$ depends on the parameter α, and the shaded region shows the available range of the permitted values for the parameters α and Q for which the event horizon exists.

In this case, the effective potential [Eq. (37)] reduces to

$$V_{\text{eff}}(r) = \left(1 - \frac{2M}{r} + \frac{Q^2}{r^2} - \alpha\right)\left(1 + \frac{L^2}{r^2}\right). \quad (47)$$

For the fixed value $M = 1$, the left column of Fig. 2 represents how the effective potential of the particles on ISCOs changes with the variation of the parameters α and Q. The second and third columns show how the specific energy and the specific angular momentum of the massive particle on the circular orbit depend on the radial coordinate, with minima appropriate to the particles on the ISCO. Table I shows the values of the specific energy, the specific angular momentum, and radius of the ISCO of a particle for the selected parameters α and Q represented in Fig. 2. Here, in this case, the ISCO is the only MSCO located on the inner border of the region of stable circular orbits, and no OSCO exists.

To find the radius of the event horizon, we solve the equation

$$N(r) = -\alpha + \frac{Q^2}{r^2} - \frac{2M}{r} + 1 = 0. \quad (48)$$

Figure 3 presents the dependence of the radius of the event horizon on different values of the parameters α and Q.

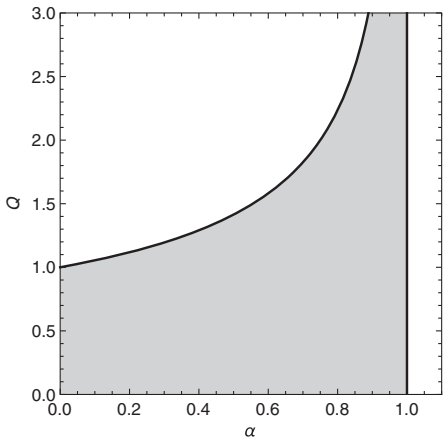

FIG. 1. Shaded region shows available range of the permitted values for the parameters α and Q for $M = 1$, allowing the existence of a black hole. Parameter α can take values in the interval $\alpha \in [0, 1)$. The parameter Q varies from 0 to $Q_{\max}$ given by the condition in Eq. (46) for the given value of the parameter α. The maximal value of the positive charge $Q_{\max}$ is represented by the solid curve on the graph.

The radius of the event horizon becomes bigger with increasing α and becomes smaller with increasing Q.

The constants of motion, specific energy E^2, and specific angular momentum L^2 given in Eqs. (43) and (44) in the case of $\omega_q = -1/3$ can be written as

$$E^2 = -\frac{(r(-2M - \alpha r + r) + Q^2)^2}{r^2(r(3M - (1-\alpha)r) - 2Q^2)}, \quad (49)$$

$$L^2 = \frac{r^2(Q^2 - Mr)}{r(3M - (1-\alpha)r) - 2Q^2}. \quad (50)$$

In Figs. 2, 4, and 5, the dependence of the radial coordinate r on E^2 and L^2 is presented.

From Eqs. (42) and (2), for the fixed value of the parameter $\omega_q = -1/3$, one can get an equation for the ISCOs:

$$f_{rms}(r) = 4Q^4 - 9MQ^2r + Mr^2[6M - (1-\alpha)r] = 0, \quad (51)$$

which has the solution

$$r_{ms} = -\frac{4M^4 - M^2[3(1-\alpha)Q^2 + 2\sqrt[3]{S}] + S^{2/3}}{(1-\alpha)M\sqrt{3S}}, \quad (52)$$

where

$$S = -8M^6 + 9(1-\alpha)M^4Q^2 - 2(1-\alpha)^2M^2Q^4 + \sqrt{R} \quad (53)$$

and

TABLE I. The specific energy, specific angular momentum, and radius of the ISCOs for the selected values of the parameters α and Q, for fixed $M = 1$.

Q	α	E^2	L^2	r_{ms}
0	0	0.8889	12	6
0.6	0	0.8785	10.7427	5.4198
0.8	0	0.8673	9.6584	4.8908
1	0	0.8437	8.0106	4.0062
0	0.3	0.6222	24.4896	8.5714
0.6	0.3	0.6174	22.7214	8.0048
0.8	0.3	0.6127	21.2539	7.5184
1	0.3	0.6050	19.2002	6.8056
0	0.6	0.3556	75	15
0.6	0.6	0.3540	71.9477	14.4455
0.8	0.6	0.3527	69.4947	13.9917
1	0.6	0.3508	66.2186	13.3735
0	0.8	0.1778	300	30
0.6	0.8	0.1774	293.949	29.453
0.8	0.8	0.1771	289.17	29.0172
1	0.8	0.1767	282.923	28.4426

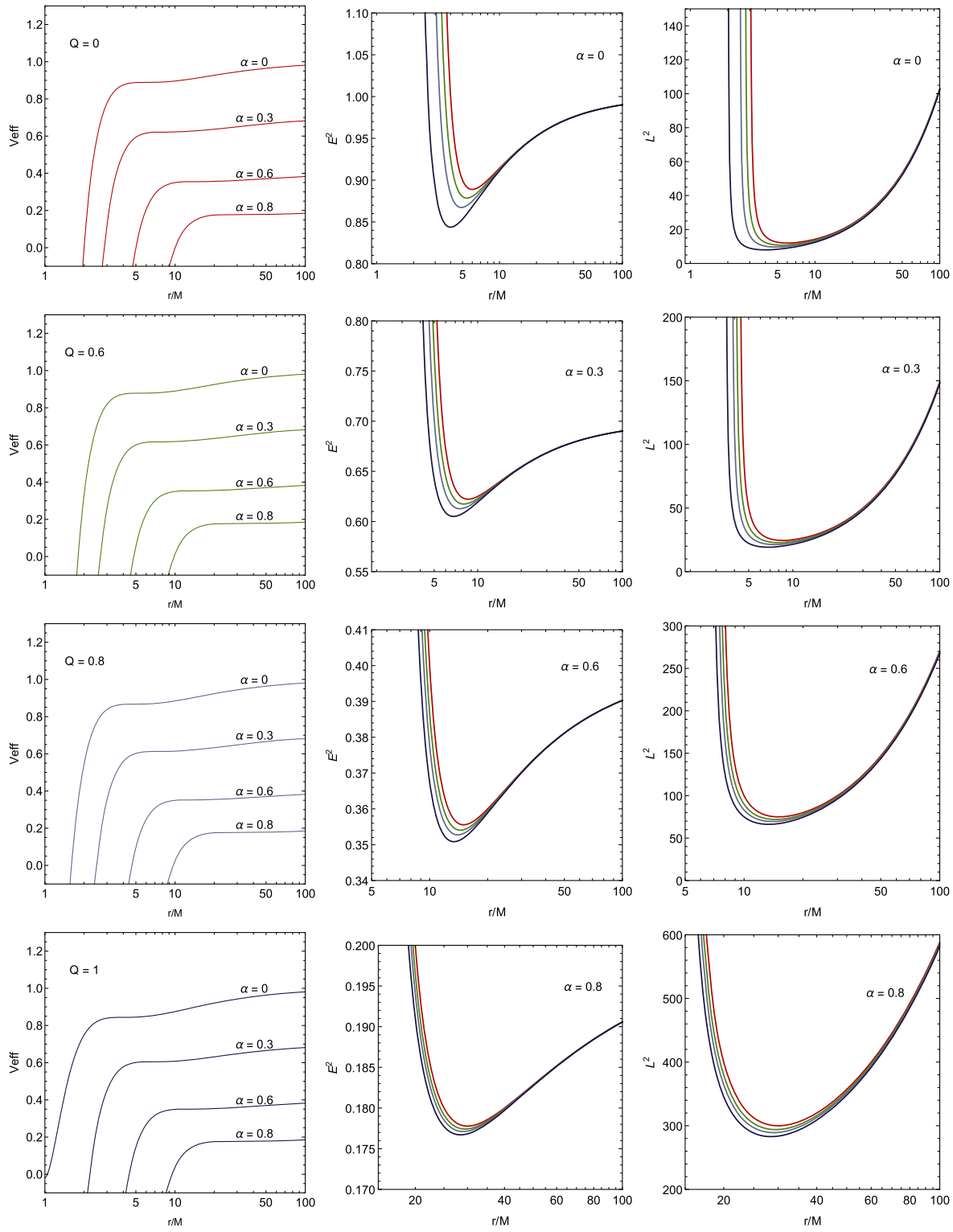

FIG. 2. The left column shows plots of the effective potentials, the central column shows the specific energy, and the right column shows the specific angular momentum of the test particle for different values of the parameters α and Q. In each row, for a chosen value of the parameter Q, four graphs for four different values of α are presented. The red color corresponds to $Q = 0$, while the green, blue, and violet colors correspond to $Q = 0.6$, $Q = 0.8$, and $Q = 1$, respectively. The parameter α takes the values $\alpha = 0$ for the first line, $\alpha = 0.3$ for the second, $\alpha = 0.6$ for the third, and $\alpha = 0.8$ for the fourth line in the graphs presented in the left column. With increasing values of α, the radii of the MSCOs also increase. The values of specific energy and the specific angular momentum for particles on ISCOs, with the radii of ISCOs, for the chosen parameters Q and α are presented in Table I.

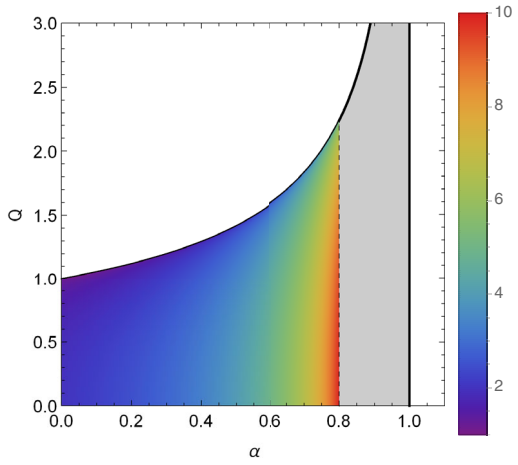

FIG. 3. Color map of the radius of the black hole event horizon for different values of the parameters α and Q, for $M = 1$. Parameter α changes from 0 to 0.8, and parameter Q changes from 0 to $Q_{\max}$ given by the condition in Eq. (46) for each value of α. For higher values of the parameter α (shown by the shaded region on the graph), the qualitative behavior of the radius of the event horizon is the same—it increases with the parameter α.

$$R = (1-\alpha)^2 M^4 Q^4 (M^2 - (1-\alpha)Q^2)(5M^2 - 4(1-\alpha)Q^2). \tag{54}$$

Radii of the ISCOs for different values of the parameters α and Q are presented in Fig. 6.

In the extremal case when energy tends to infinity, the radius of the ISCO coincides with the radius of the circular photon orbit. We can get the radii of photon circular orbits by requiring that the energy in Eq. (49) go to infinity, and then solving the equation

$$f_{rph}(r) = r(3M - (1-\alpha)r) - 2Q^2 = 0, \tag{55}$$

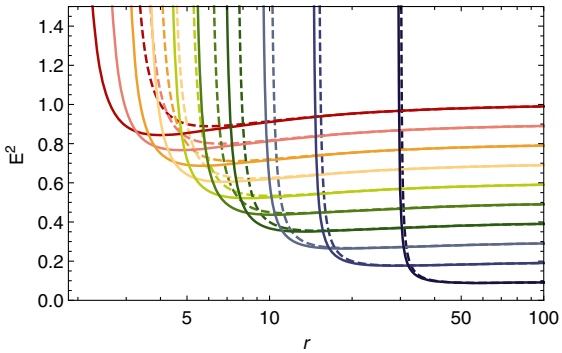

FIG. 4. Plots of the square of the specific energy, E^2, for different values of the parameters α and Q, for $M = 1$. Here α increases from red to violet colors and takes the values $\alpha = \{0, 0.1, 0.2, 0.3, 0.4, 0.5, 0.6, 0.7, 0.8, 0.9\}$, respectively. For each value of α, Q takes two characteristic values: $Q = 0$ for dashed lines and $Q = 1$ for solid lines.

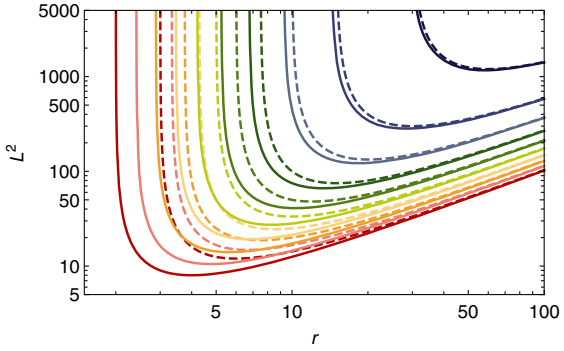

FIG. 5. Plot of the specific angular momentum, L^2, for different values of α and Q, for $M = 1$. Here α increases from red to violet colors and takes the values $\alpha = \{0, 0.1, 0.2, 0.3, 0.4, 0.5, 0.6, 0.7, 0.8, 0.9\}$, respectively. For each value of α, Q takes two characteristic values: $Q = 0$ for dashed lines and $Q = 1$ for solid lines.

which has the following solution:

$$r_{ph} = \frac{\sqrt{9M^2 - 8(1-\alpha)Q^2} + 3M}{2(1-\alpha)}. \tag{56}$$

Figure 7 presents the radius of the photon circular orbit with varying parameters α and Q.

In order to show how the radius of the ISCO of massive particles, the radius of the photon orbit, and the radii of the horizons depend on the parameter α, we express α as a function of the radial coordinate r of the spacetime horizons, the ISCO, and circular photon orbit from Eqs. (48), (55), and (51). From Eq. (48), which defines the radii of the spacetime horizons, one can express the parameter α as a function of r in the following form:

$$\alpha_h(r) = \frac{-2Mr + Q^2 + r^2}{r^2}. \tag{57}$$

From Eq. (55), which defines the radius of the photon orbit, one can express the parameter α as a function of r:

$$\alpha_{rph}(r) = \frac{-3Mr + 2Q^2 + r^2}{r^2}. \tag{58}$$

Similarly, from Eq. (51), which defines the radius of the ISCO, one can express the parameter α as a function of r and Q in the following way:

$$\alpha_{ms}(r) = -\frac{6M^2r^2 - 9MQ^2r - Mr^3 + 4Q^4}{Mr^3}. \tag{59}$$

Figure 8 for the presented values of the parameter Q allows us to determine the radii of the horizons, the radius of the ISCO, and the radius of the photon orbit for different values of the parameter α; also, from Fig. 8, it is possible to determine the region where stable circular orbits exist

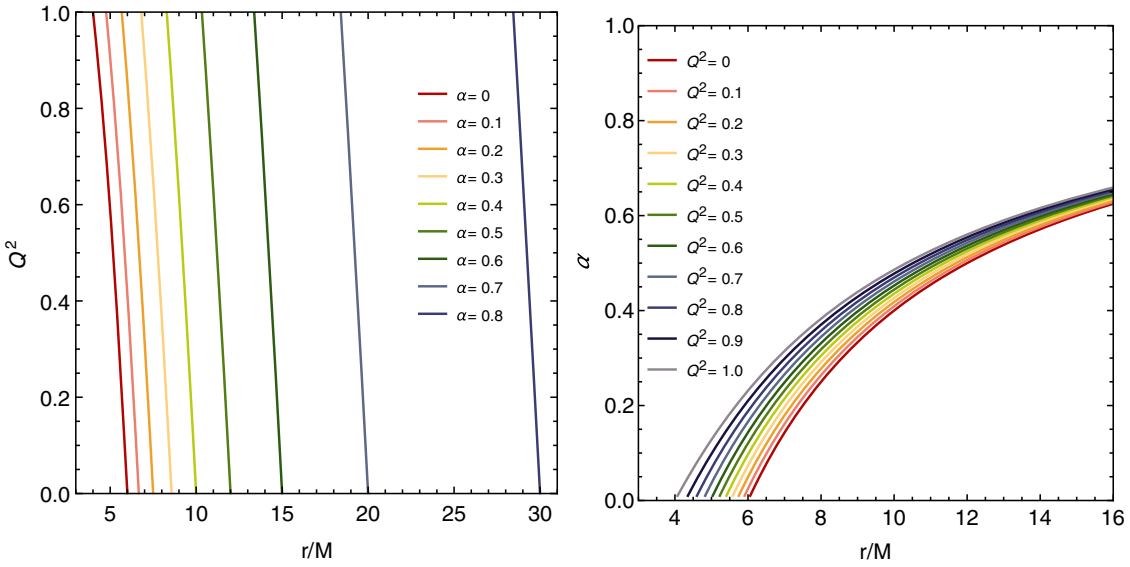

FIG. 6. The left graph shows how the radii of ISCOs depend on Q for some different fixed values of $\alpha = \{0, 0.1, \ldots, 0.8\}$. The right graph shows how the radii of ISCOs depend on α for some different fixed values of Q in the range from $Q = 0$ to $Q = 1$.

and at what values of α, for a given Q, the event horizon disappears.

B. MSCOs around the charged Kiselev black hole with $\omega_q = -2/3$

In this section, we explore the motion of particles when the parameter $\omega_q = -2/3$. In this case, the lapse function $N(r)$ takes the following form:

$$N(r) = -\alpha r + \frac{Q^2}{r^2} - \frac{2M}{r} + 1. \tag{60}$$

One can find the radii of the horizons by solving the following equation:

$$-\alpha r + \frac{Q^2}{r^2} - \frac{2M}{r} + 1 = 0. \tag{61}$$

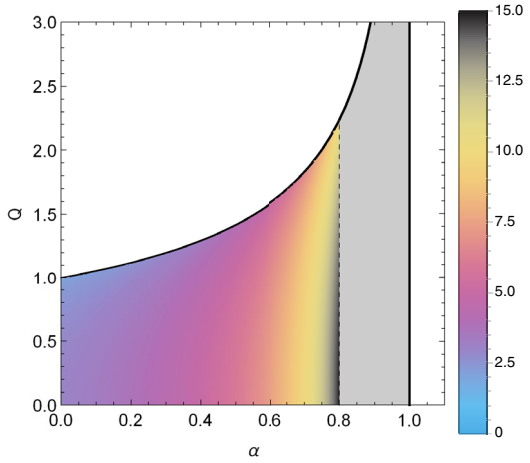

FIG. 7. Color map demonstrates the radii of photon orbits for different values of the parameters α and Q, for $M = 1$. Parameter α takes values from 0 to 0.8, and parameter Q ranges from 0 to $Q_{\max}$ given by the condition in Eq. (46) for each value of the parameter α.

Figure 9 demonstrates the radius of the black hole event horizon for different values of the parameters α and Q.

In this case, the event horizon exists only for some limited values of the charge Q; for the maximum value of the charge, the parameter α is related with the parameter Q by the conditions $0 \leq \alpha < \alpha_+$ if $0 \leq Q < 1$, and $\alpha_- \leq \alpha < \alpha_+$ if $Q \geq 1$, where $\alpha_\pm$ is equal to

$$\alpha_\pm(Q) = \frac{r_\pm^2 - 2Mr_\pm + Q^2}{r_\pm^3} \tag{62}$$

and

$$r_\pm(Q) = 2M \pm \sqrt{4M^2 - 3Q^2}. \tag{63}$$

Figure 10 shows the upper limit on the parameter α for which the event horizon exists. Figure 11 shows the upper limit on the parameter α for which MSCOs exist.

In this case, the effective potential [Eq. (37)] reduces to

$$V_{\text{eff}} = \left(1 - \frac{2M}{r} + \frac{Q^2}{r^2} - \alpha r\right)\left(1 - \frac{L^2}{r^2}\right). \tag{64}$$

The effective potential for several values of parameters α and Q is shown in Fig. 12.

The squares of the constants of motion E^2 and L^2 given in Eqs. (43) and (44), in the case of $\omega_q = -2/3$, can be written as

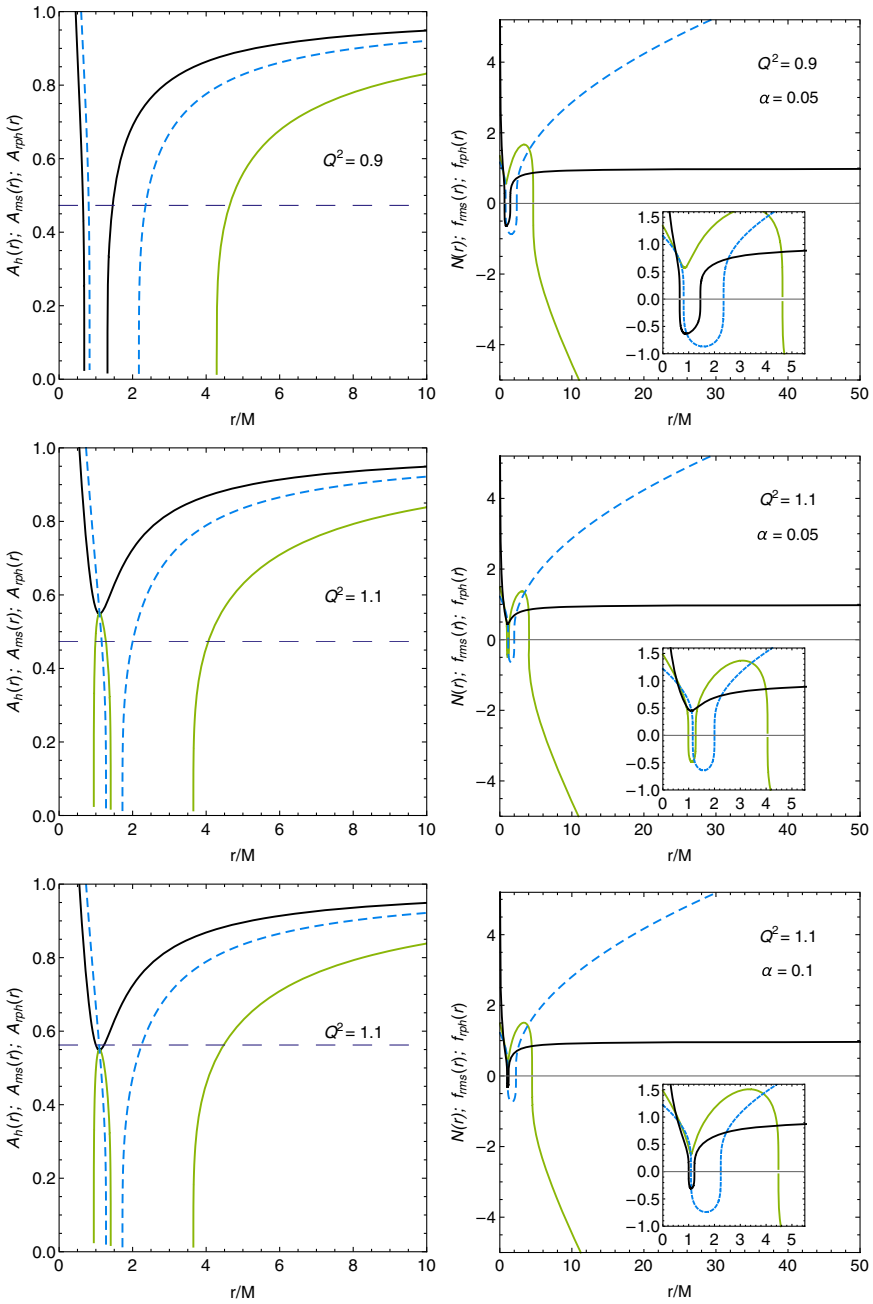

FIG. 8. Plots in the left column show the radial dependence of functions $\alpha_h(r)$, $\alpha_{ms}(r)$, and $\alpha_{rph}(r)$ [Eqs. (57), (59) and (58) in the text] for several values of the charge Q with the fixed value of $M = 1$. For better visualization, instead of the functions themselves on the plots, we show $A_h(r) = Sgn(\alpha_h(r))|\alpha_h(r)|^{1/4}$, $A_{ms}(r) = Sgn(\alpha_{ms}(r))|\alpha_{ms}(r)|^{1/4}$, and $A_{rph}(r) = Sgn(\alpha_{rph}(r))|\alpha_{rph}(r)|^{1/4}$. The thin black line is the graph of the function $A_h(r)$, which determines the positions of the event horizons. The blue dashed line is the graph of the function $A_{rph}(r)$, which determines the positions of the photon orbits. The thin green line is the graph of the function $A_{ms}(r)$, which determines the positions of the stable circular orbits. The gray dashed line defines the parameter $\alpha^{1/4}$, for which the functions $N(r)$, $f_{rph}(r)$, and $f_{rms}(r)$ are shown in the right column. In the right column, for some parameters α and Q, the following graphs are presented: The thin black line is a graph of the function $N(r)$ [Eq. (48) in the text]; zero values of this function determine the positions of the horizons for the selected values of the parameter α. The blue dashed line is a graph of the function $f_{rph}(r)$, [Eq. (55) in the text]; zero values of this function determine the position of the photon orbit for the selected values of the parameter α. The thin green line is a graph of function $f_{rms}(r)$ [Eq. (51) in the text]; zero values of this function determine the position of the ISCO for the selected values of the parameter α. Parameters α and Q take the values $\alpha = [0.05, 0.1]$ and $Q = [0.9, 1.1]$.

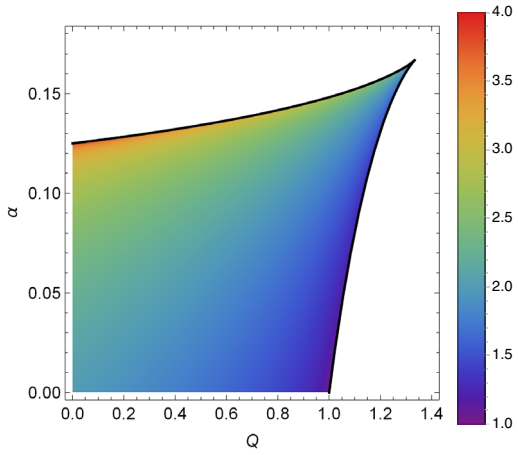

FIG. 9. Color map of the radius of the event horizon for different values of the parameters α and Q, for $M = 1$. The parameter α varies from 0 to α_+ if $0 \leq Q < 1$, and from α_- to α_+ if $Q \geq 1$ ($\alpha_{\max} = 1/6$ and $Q_{\max} = 3/4$). For the white regions, there is no event horizon in the spacetime, and they correspond to the naked singularity. The region where the event horizon exists is given by the condition in Eq. (62).

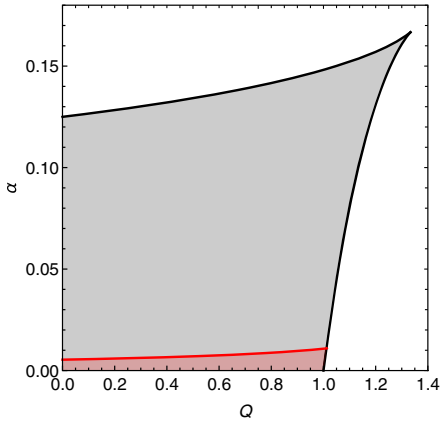

FIG. 10. The gray shaded region shows the allowable range of the parameters α and Q for which the event horizon exists. Parameter α takes values from 0 to α_+ if $0 \leq Q < 1$, and $\alpha_- \leq \alpha < \alpha_+$ if $Q \geq 1$; the value of $\alpha_\pm$ is given by the condition in Eq. (62).

$$E^2 = \frac{2\left(\frac{r(r-2M)+Q^2}{r^2} - \alpha r\right)^2}{\frac{2(r(r-3M)+2Q^2)}{r^2} - \alpha r}, \tag{65}$$

$$L^2 = \frac{2(Mr - Q^2) - \alpha r^3}{\frac{2(r(r-3M)+2Q^2)}{r^2} - \alpha r}. \tag{66}$$

Figures 12–14 provide the dependence of the radial coordinate r on E^2 and L^2.

Tables II and III show the specific energy and angular momentum of a particle in the ISCO and OSCO for the selected values of the parameters α and Q.

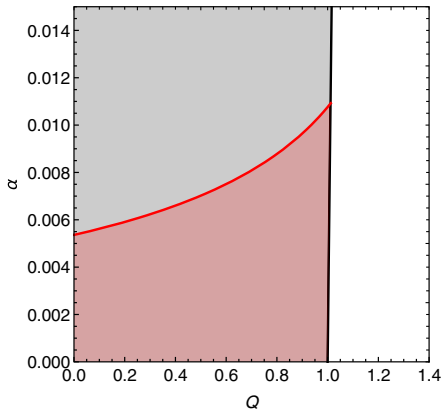

FIG. 11. The red shaded region shows the allowable range of the parameters α and Q for which the MSCOs exist. The parameter α takes values from 0 to α_{ms+} if $0 \leq Q < 1$, and $\alpha_- \leq \alpha < \alpha_{ms+}$ if $Q \geq 1$.

Now, using Eq. (39), one can get the condition for a static radius:

$$f_{rst}(r) = \alpha r^3 - 2Mr + 2Q^2 = 0. \tag{67}$$

From Eqs. (42) and (2), for the fixed value of the parameter $\omega_q = -2/3$, we get the following equation for the radii of MSCOs:

$$f_{rms}(r) = Q^2(18Mr - 11\alpha r^3) - 3\alpha r^4(r - 4M) + 2Mr^2(r - 6M) - 8Q^4 + \alpha^2 r^6 = 0. \tag{68}$$

The radii of ISCOs for different values of the parameters α and Q are presented in Fig. 15:

The radius of the photon orbit can be obtained from the equation for the specific energy [Eq. (65)], which for the particles in the photon orbit goes to infinity:

$$f_{rph}(r) = \frac{2(r(r-3M)+2Q^2)}{r^2} - \alpha r = 0. \tag{69}$$

Figure 16 shows the color map for the photon orbit for different values of the parameters α and Q.

In order to show how the ISCOs and OSCOs of massive particles, the radius of the photon orbit, the radius of the event horizon, and the static radius depend on α, we express the parameter α as a function of radial coordinate r from the equations that correspond to these values: Eqs. (68), (69), (61), and (67).

From Eq. (61), one can express the parameter α as a function of the radial coordinate r and the black hole charge Q in the following form:

$$\alpha_h(r) = \frac{-2Mr + Q^2 + r^2}{r^3}. \tag{70}$$

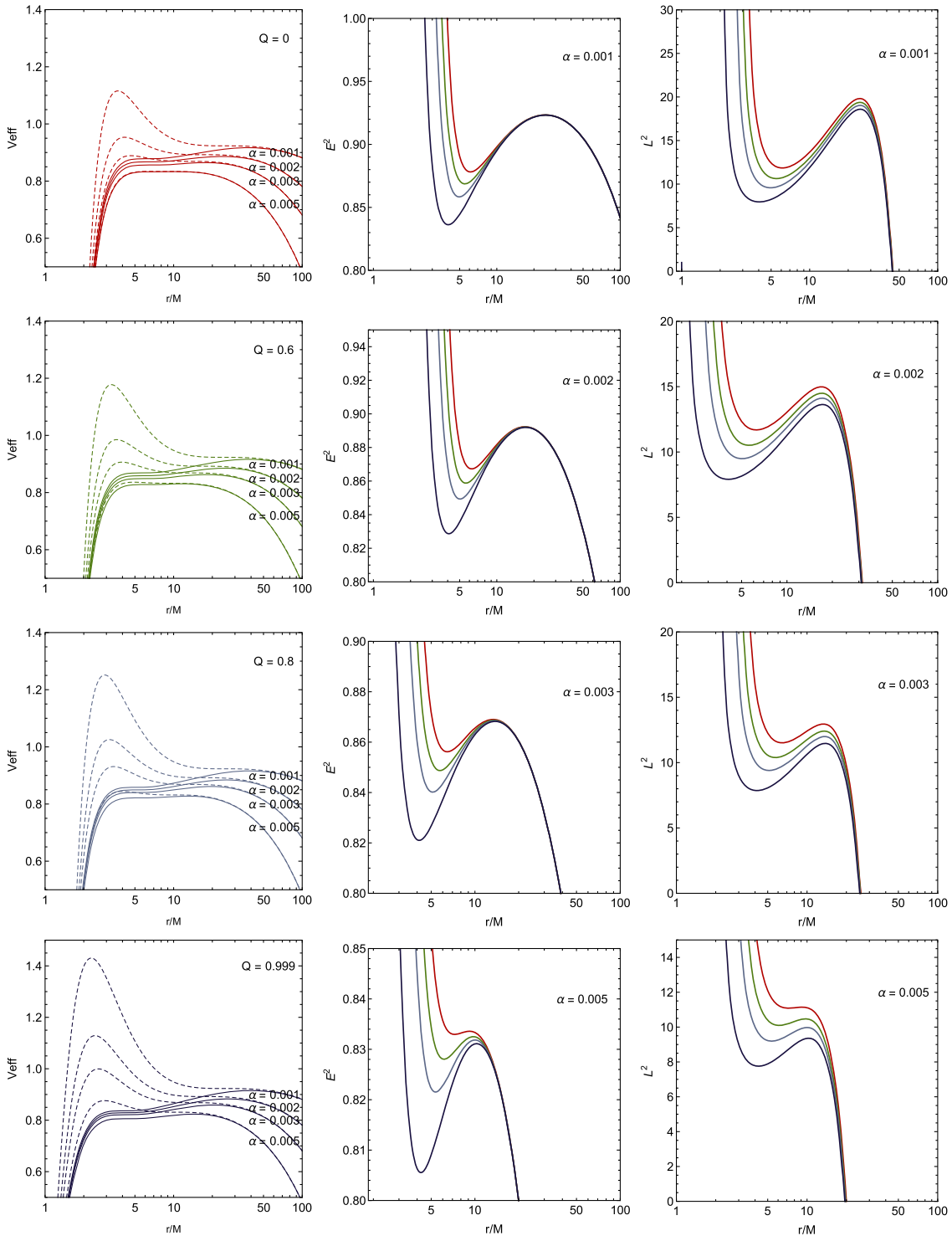

FIG. 12. The left column shows plots of the effective potentials, the central column shows the specific energy, and the right column shows the specific angular momentum of the test particle for different values of the parameters α and Q. In each row, for a chosen value of the parameter Q, eight graphs for four different values of α are presented. The red color corresponds to $Q = 0$, while the green, blue, and violet colors correspond to $Q = 0.6$, $Q = 0.8$, and $Q = 0.999$, respectively. The parameter α takes the values $\alpha = 0.001$ for the first line, $\alpha = 0.002$ for the second, $\alpha = 0.003$ for the third, and $\alpha = 0.005$ for the fourth line in the graphs presented in the left column. In the first column, solid lines represent the effective potential of the particles in the ISCOs, and dashed lines represent the effective potential of the particles in the OSCOs. With increasing values of α, the radii of the ISCOs also increase, and the radii of the OSCOs decrease. The values of specific energy and the specific angular momentum for particles on MSCOs, with the radii of MSCOs, for chosen parameters Q and α are presented in Tables II and III.

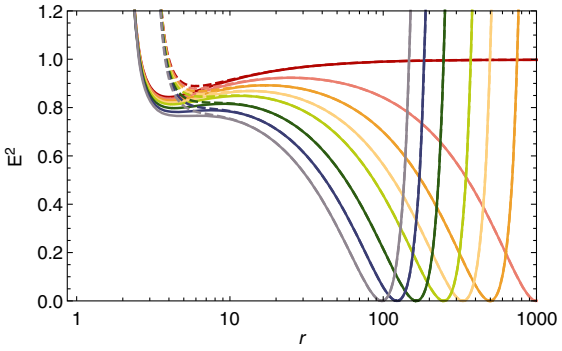

FIG. 13. Plot of E^2 for different values of the parameters α and Q. Here α increases from the red color to the violet one and takes the values $\alpha = \{0, 0.001, 0.002, 0.003, 0.004, 0.006, 0.008, 0.01\}$, respectively. For each value of α, Q takes two characteristic values: $Q = 0$ for dashed lines and $Q = 1$ for solid lines.

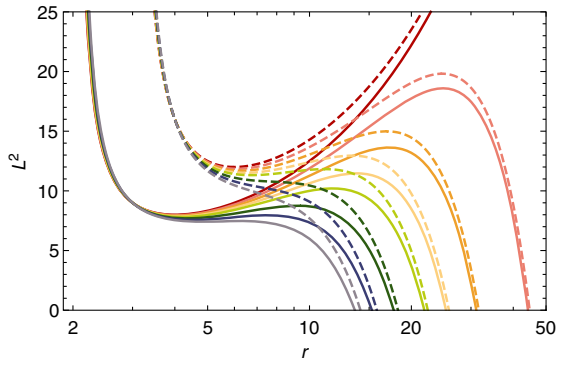

FIG. 14. Plot of L^2 for different values of α and Q. Here α increases from the red color to the violet color and takes the values $\alpha = \{0, 0.001, 0.002, 0.003, 0.004, 0.006, 0.008, 0.01\}$, respectively. For each value of α, Q takes two characteristic values: $Q = 0$ for dashed lines and $Q = 1$ for solid lines.

From Eq. (69), one can express the parameter α as a function of the radial coordinate r and the black hole charge Q in the following manner:

$$\alpha_{rph}(r) = \frac{2(r(r-3M)+2Q^2)}{r^3}. \tag{71}$$

From Eq. (68), one can express the parameter α as a function of the radial coordinate r and the black hole charge Q in the following way:

$$\alpha_{ms}(r) = \frac{-(192M^2r^2 - 336MQ^2r - 80Mr^3)^{1/2}}{2r^3} \times (153Q^4 + 66Q^2r^2 + 9r^4)^{1/2} - \frac{12Mr + 11Q^2 + 3r^2}{2r^3}. \tag{72}$$

From Eq. (67), one can express the parameter α as a function of the radial coordinate r and the black hole charge Q in the following form:

TABLE II. The specific energy, angular momentum, and radius of the ISCO of the test particle for selected values of the parameters α and Q, for fixed $M = 1$.

Q	α	E^2	L^2	r_{ms}
0	0.001	0.8782	11.8509	6.1182
0.6	0.001	0.8687	10.6325	5.5079
0.8	0.001	0.8583	9.5769	4.9571
0.999	0.001	0.8364	7.9667	4.0471
0	0.002	0.8673	11.6902	6.2633
0.6	0.002	0.8588	10.5147	5.6116
0.8	0.002	0.8493	9.4909	5.0328
0.9991	0.002	0.8288	7.9206	4.0918
0	0.003	0.8562	11.5145	6.4513
0.6	0.003	0.8487	10.388	5.7377
0.8	0.003	0.8402	9.3993	5.12095
0.999	0.003	0.8212	7.8721	4.1411
0	0.005	0.833	11.0852	7.2378
0.6	0.005	0.828	10.0967	6.1268
0.8	0.005	0.8215	9.1950	5.3589
0.999	0.005	0.8057	7.7667	4.2583

TABLE III. The specific energy, angular momentum, and radius of the OSCO of the test particle for selected values of the parameters α and Q, for fixed $M = 1$.

Q	α	E^2	L^2	r_{ms}
0	0.001	0.92337	19.8171	24.6596
0.6	0.001	0.92334	19.3751	24.717
0.8	0.001	0.92331	19.0322	24.7601
0.999	0.001	0.92327	18.5952	24.8133
0	0.002	0.89235	14.9869	16.9089
0.6	0.002	0.89221	14.4953	17.015
0.8	0.002	0.89211	14.1158	17.0918
0.999	0.002	0.89199	13.6341	17.1837
0	0.003	0.86901	12.9507	13.3434
0.6	0.003	0.86871	12.4093	13.5159
0.8	0.003	0.86849	11.9944	13.6345
0.999	0.003	0.86824	11.4708	13.77
0	0.005	0.83359	11.1433	9.1628
0.6	0.005	0.83251	10.4704	9.7385
0.8	0.005	0.83184	9.9738	10.0128
0.999	0.005	0.83113	9.3619	10.2751

$$\alpha_{rst}(r) = -\frac{2(Q^2 - Mr)}{r^3}. \tag{73}$$

Figure 17 allows us to determine the existence of an event horizon, stable circular orbits, photon orbit, and static radius for three values of Q and certain values of α. If the choice of parameters allows the existence of these quantities, then it is possible to determine the corresponding radii from Fig. 17.

For each value of the parameter Q, there is a maximum value of the parameter $\alpha_{ms+}(Q)$, which defines the region

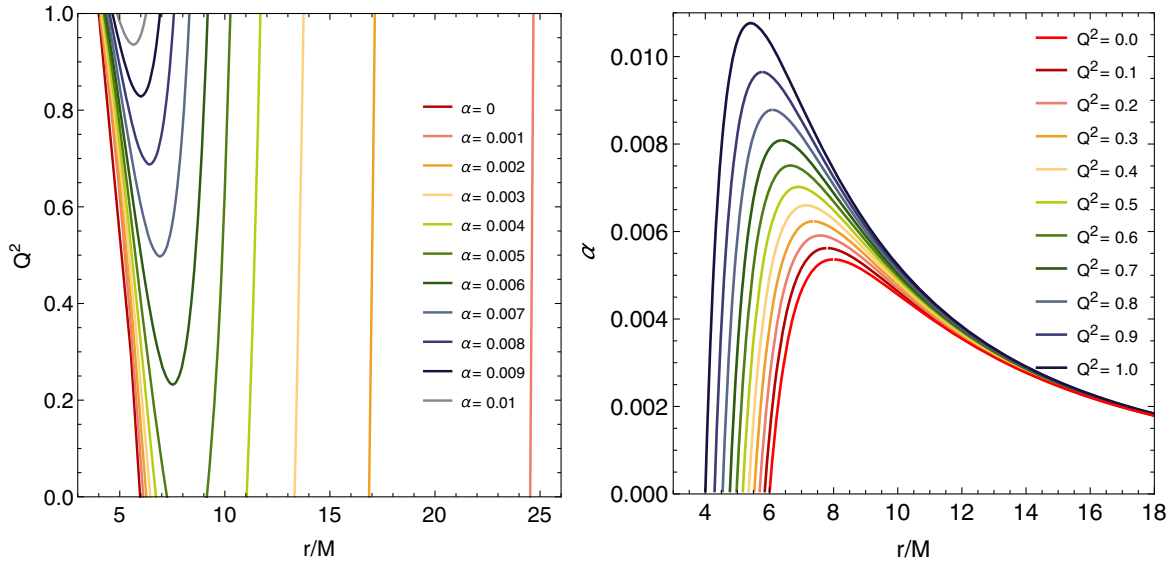

FIG. 15. In the left plot, the dependence of the radii of the ISCO and OSCO for the whole range of Q^2 is shown; each graph is for different values of α, from $\alpha = 0$ to $\alpha = 0.01$. In the right plot, the dependence of the radii of the ISCO and OSCO for the whole range of α is shown; each graph corresponds to different values of Q^2, from $Q^2 = 0$ to $Q^2 = 1.0$.

of stable circular orbits. Taking the derivative with respect to r from Eq. (72) for $\alpha_{ms}(r)$ and equating the resulting expression to 0, one can obtain the value of $r_{\rm crit}$ that determines the radius of a stable circular orbit for values of the parameter Q from 0 to $Q_{\rm max}$. Substituting the obtained value of $r_{\rm crit}$ for a given Q into Eq. (72) for $\alpha_{ms}(r)$, we obtain the maximum value of the parameter $\alpha_{ms+}(Q)$ for a stable circular orbit for the given value of Q. The thick red line in Fig. 11 shows the dependence of the maximum value for the parameter α on Q, and the shaded area under the thick red line in Fig. 11 determines the values of the parameters α and Q for which stable circular orbits exist.

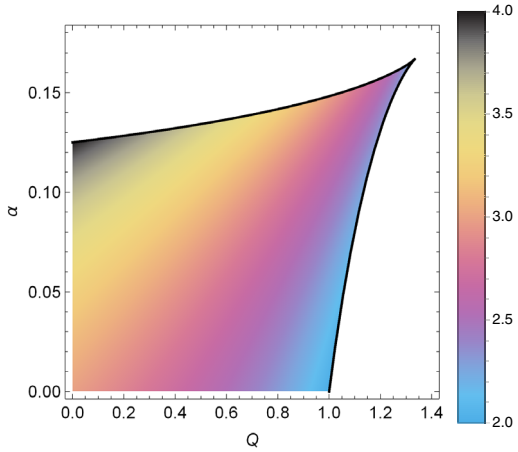

FIG. 16. Color map shows the radii of photon orbits for different values of the parameters α and Q. The parameter α takes values from 0 to α_+ if $0 \le Q < 1$, and $\alpha_- \le \alpha < \alpha_+$ if $Q \ge 1$; the value of $\alpha_\pm$ is given by the condition in Eq. (62).

C. MSCOs around the charged Kiselev black hole with $\omega_q = -1$ (the cosmological constant)

In this section, we study particles' motion when the parameter $\omega_q = -1$. The lapse function [Eq. (2)] in this case takes the following form:

$$N(r) = 1 - \frac{2M}{r} - \alpha r^2 + \frac{Q^2}{r^2}. \tag{74}$$

The radii of the event horizons can be obtained by solving the equation

$$1 - \frac{2M}{r} - \alpha r^2 + \frac{Q^2}{r^2} = 0. \tag{75}$$

Figure 18 demonstrates the dependence of the radius of the black hole event horizon on different values of the parameters α and Q.

By analyzing the behavior of the function (75), it is possible to find the restrictions on the parameters α and Q that are appropriate for the black hole spacetime. In Ref. [35], it was shown that for the Reissner-Nordström spacetime with a nonzero cosmological constant, the solutions are

$$\alpha_{h(\max)}(Q) \equiv \frac{M r_{e(h)+} - Q^2}{r_{e(h)+}^4}, \tag{76}$$

and

$$\alpha_{h(\min)}(Q) \equiv \frac{M r_{e(h)-} - Q^2}{r_{e(h)-}^4}, \tag{77}$$

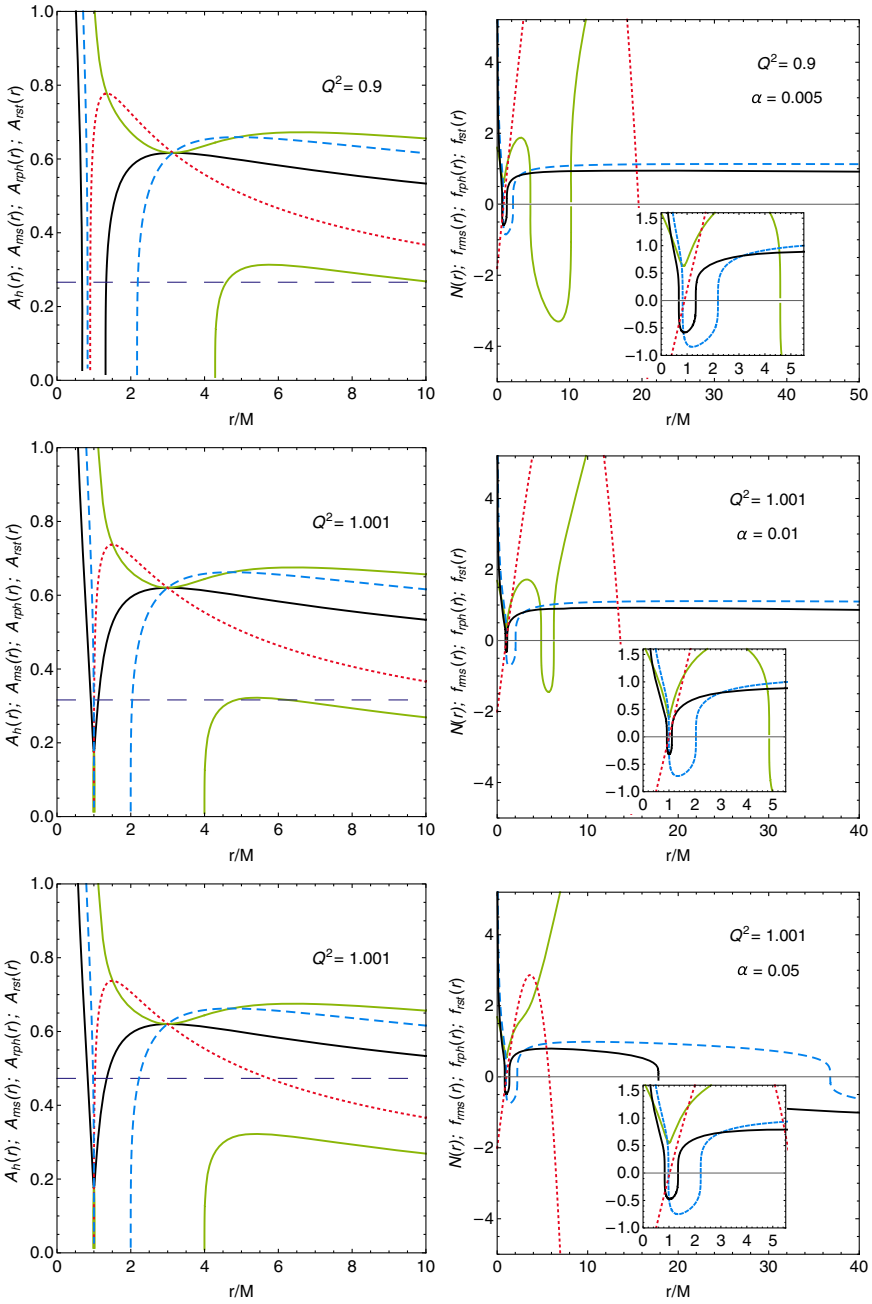

FIG. 17. Plots in the left column show the radial dependences of the functions $\alpha_h(r)$, $\alpha_{rst}(r)$, $\alpha_{ms}(r)$, and $\alpha_{rph}(r)$ [Eqs. (70), (73), (72), and (71) in the text] for several values of the parameter Q with fixed $M = 1$. For better visualization, instead of the functions themselves in the plots, we show $A_h(r) = Sgn(\alpha_h(r))|\alpha_h(r)|^{1/4}$, $A_{rst}(r) = Sgn(\alpha_{rst}(r))|\alpha_{rst}(r)|^{1/4}$, $A_{ms}(r) = Sgn(\alpha_{ms}(r))|\alpha_{ms}(r)|^{1/4}$, and $A_{rph}(r) = Sgn(\alpha_{rph}(r))|\alpha_{rph}(r)|^{1/4}$. The thin black line is the graph of the function $A_h(r)$, which determines the positions of the event horizons. The blue dashed line is the graph of the function $A_{rph}(r)$, which determines the position of the photon orbit. The thin green line is the graph of the function $A_{ms}(r)$, which determines the positions of the stable circular orbits. The red dotted line is the graph of the function $A_{rst}(r)$, which determines the position of the static radius. The gray dashed line defines the parameter $\alpha^{1/4}$, for which the functions $N(r)$, $f_{rph}(r)$, $f_{rst}(r)$, and $f_{rms}(r)$ are shown in the right column. In the right column, for some values of the parameters α and Q, the following graphs are presented: The thin black line is the graph of the function $N(r)$ [Eq. (60)]; zero values of this function determine the positions of the horizons for the selected values of the parameter α. The blue dashed line is the graph of the function $f_{rph}(r)$ [Eq. (69)]; zero values of this function determine the position of the photon orbit for the selected values of the parameter α. The thin green line is the graph of the function $f_{rms}(r)$ [Eq. (68)]; zero values of this function determine the position of the ISCO for the selected values of the parameter α. The red dotted line is the graph of the function $f_{rst}(r)$ [Eq. (67)]; zero values of the function determine the position of the static radius for the selected values of the parameter α. Parameters α and Q take the values $\alpha = [0.05, 0.001, 0.005]$ and $Q = [0.9, 1.001]$.

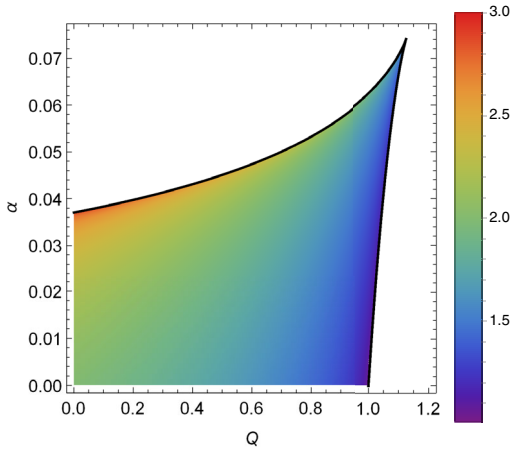

FIG. 18. Color map of the radius of the event horizon for different values of the parameters α and Q. Parameter Q changes from 0 to $Q_{\max}$, and parameter α takes values from 0 to $\alpha_{h(\max)}$ if $0 \leq Q < 1$, and $\alpha_{h(\min)} \leq Q < \alpha_{h(\max)}$ if $Q \geq 1$. The functions $\alpha_{h(\min)}$ and $\alpha_{h(\max)}$ are given by the conditions in Eqs. (77) and (76) for each value of Q.

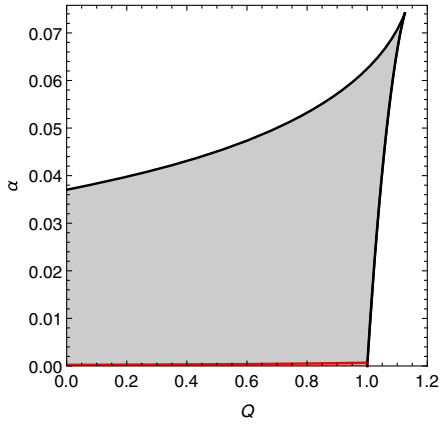

FIG. 19. The black line limits the interval of the variation of the parameters α and Q in which the existence of black hole spacetime is allowed. The parameters α and Q lying outside the region confined by the black line are consistent with naked singularities. Parameter α takes values $0 \leq \alpha < \alpha_{h(\max)}$ if $Q < 1$ and $\alpha_{h(\min)} \leq \alpha < \alpha_{h(\max)}$ if $Q \geq 1$. The functions $\alpha_{h(\min)}(Q)$ and $\alpha_{h(\max)}(Q)$ are given by the conditions in Eqs. (76) and (77).

where

$$r_{e(h)\pm} = \frac{3}{2}\left[M \pm \left(M^2 - \frac{8Q^2}{9}\right)^{1/2}\right]. \tag{78}$$

The maximum value of the parameter α which allows the existence of the black hole solution corresponds to the maximum value of the charge $Q_{\max} = \sqrt{9/8}$ and is equal to

$$\alpha = \alpha_{\max} \equiv \frac{2}{27}. \tag{79}$$

Figure 19 shows the range of acceptable values of the parameters α and Q for the existence of a black hole.

We study only black holes with asymptotically de Sitter behavior, and for this reason we imply that $\alpha > 0$ for $0 < Q \leq 1$, and $\alpha = \alpha_{h(\min)}$ for $1 < Q \leq \sqrt{9/8}$.

Using Eq. (39), we get the condition for a static radius:

$$f_{rst}(r) = \alpha r^4 - Mr + Q^2 = 0. \tag{80}$$

Then the effective potential [Eq. (37)] takes the following form:

$$V_{\text{eff}} = \left(1 - \frac{2M}{r} + \frac{Q^2}{r^2} - \alpha r^2\right)\left(1 - \frac{L^2}{r^2}\right). \tag{81}$$

The effective potential for several values of parameters α and Q is shown in Fig. 21.

The constants of motion E^2 and L^2, given in Eqs. (43) and (44), in this case can be written as

$$E^2 = \frac{r^4\left(\frac{r(r-2M)+Q^2}{r^3} - \alpha r\right)^2}{r(r-3M)+2Q^2}, \tag{82}$$

$$L^2 = \frac{r^3\left(\frac{2(Mr-Q^2)}{r} - 2\alpha r^3\right)}{2(r(r-3M)+2Q^2)}. \tag{83}$$

Figures 22, 23, and 26 illustrate the dependence of E^2 and L^2 on the radial coordinate r.

Tables IV and V show the specific energy and angular momentum of a particle in the ISCO and the OSCO for the selected parameters α and Q.

In the same way as it was done in the previous sections, we can get the radius of the photon circular orbit by

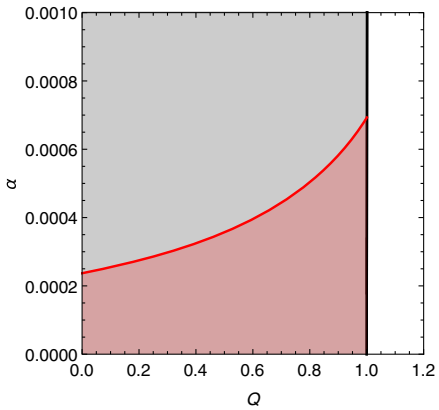

FIG. 20. The red line limits the range of parameters α and Q for which stable circular orbits exist. The values of the parameter α in the case of $Q > 1$ are also bounded from below by the minimum value of the parameter $\alpha_{h(\min)}$ for which there is a black hole event horizon.

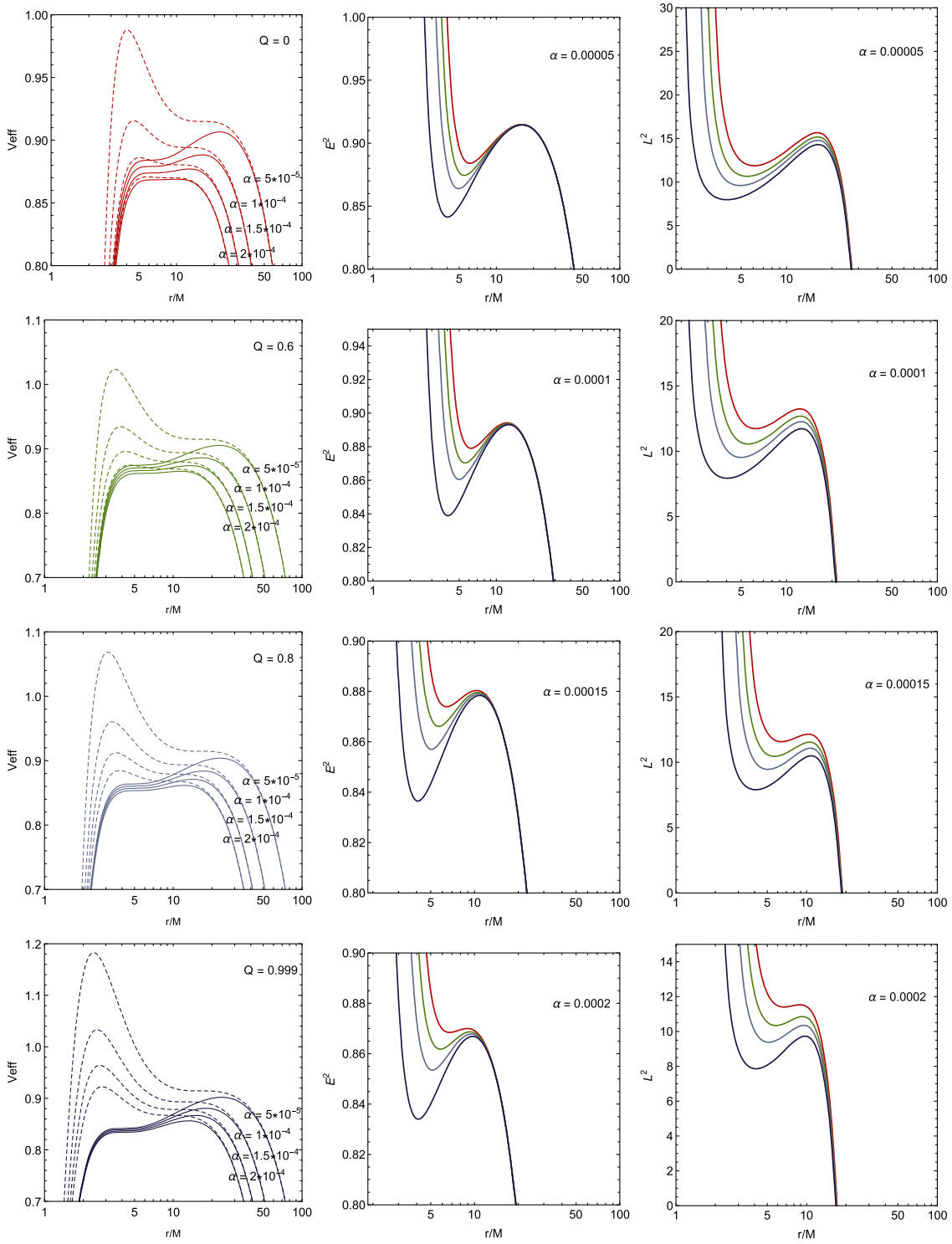

FIG. 21. The left column shows plots of effective potentials, the central column shows the specific energy, and the right column shows the specific angular momentum of the test particle for different values of parameters α and Q. In each row, for chosen values of the parameter Q, eight graphs are presented for four different values of α. The red color corresponds to $Q = 0$, while the green, blue, and violet colors correspond to $Q = 0.6$, $Q = 0.8$, and $Q = 0.999$, respectively. Parameter α takes the values $\alpha = 0.00005$ for the first line, $\alpha = 0.0001$ for the second, $\alpha = 0.00015$ for the third, and $\alpha = 0.0002$ for the fourth line in the graphs presented in the left column. In the first column, solid lines represent the effective potential of the particles on the ISCOs, and dashed lines represent the effective potential of the particles on the OSCOs. With increasing values of α, the radii of ISCOs also increase, but the radii of OSCOs decrease. The values of specific energy and the specific angular momentum for particles in MSCOs, with the radii of MSCOs for chosen parameters Q and α, are presented in Tables IV and V.

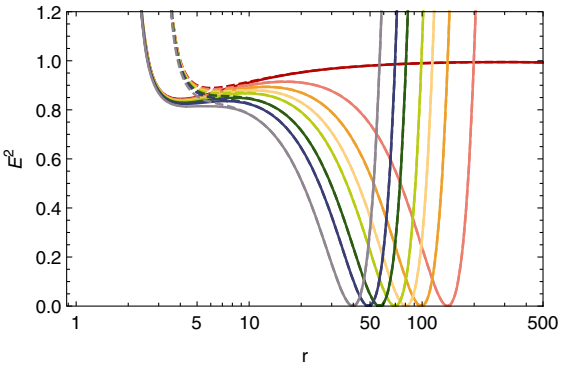

FIG. 22. Plot of the specific energy E^2 for different values of parameters Q and α. Here α increases from the red color to the violet color and takes the values $\alpha = \{0, 0.00005, 0.0001, 0.00015, 0.0002, 0.0003, 0.0004, 0.0006\}$, respectively. For each value of α, Q takes two characteristic values: $Q = 0$ for dashed lines and $Q = 1$ for solid lines. Parameter M is fixed and equals 1.

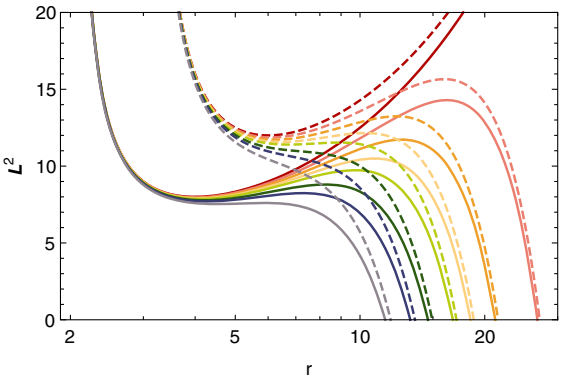

FIG. 23. Plot of the specific angular momentum L^2 for different values of α and Q. Here α increases from the red color to the violet one and takes the values $\alpha = \{0, 0.00005, 0.0001, 0.00015, 0.0002, 0.0003, 0.0004, 0.0006\}$, respectively. For each value of α, Q takes two characteristic values: $Q = 0$ for dashed lines and $Q = 1$ for solid lines. Parameter M is fixed and equals 1.

requiring the energy in Eq. (82) to go to infinity, and solving the equation

$$f_{rph}(r) = r(r - 3M) + 2Q^2 = 0, \tag{84}$$

we have

$$r_{ph} = \frac{1}{2}\left(3M \pm \sqrt{9M^2 - 8Q^2}\right). \tag{85}$$

From Eq. (85), it is clear that photon orbits do not depend on α. In Fig. 24, the dependence of the radius of the photon circular orbit on the parameters α and Q is shown.

From Eqs. (42) and (2), for the fixed value of the parameter $\omega_q = -1$ we get the following equation for radii of the MSCO:

TABLE IV. The specific energy, angular momentum, and radius of the test particle in the ISCO for some values of the parameters α and Q, for fixed $M = 1$.

Q	α	E^2	L^2	r_{ms}
0	0.00005	0.88403	11.867	6.10741
0.6	0.00005	0.87444	10.6497	5.4914
0.8	0.00005	0.86391	9.5925	4.9389
0.999	0.00005	0.84152	7.9761	4.0298
0	0.0001	0.87904	11.7258	6.2425
0.6	0.0001	0.87032	10.5523	5.5756
0.8	0.0001	0.86049	9.5246	4.9932
0.999	0.0001	0.83909	7.9409	4.0551
0	0.00015	0.87387	11.5732	6.4261
0.6	0.00015	0.86611	10.45	5.6782
0.8	0.00015	0.85702	9.4544	5.0554
0.999	0.00015	0.83665	7.9052	4.0824
0	0.0002	0.86842	11.4026	6.7224
0.6	0.0002	0.86177	10.3412	5.8101
0.8	0.0002	0.85348	9.3814	5.1282
0.999	0.0002	0.83418	7.8688	4.1118

TABLE V. The specific energy, angular momentum, and radius of the test particle in the OSCO for some values of the parameters α and Q, for fixed $M = 1$.

Q	α	E^2	L^2	r_{ms}
0	0.00005	0.91494	15.6594	15.9792
0.6	0.00005	0.91476	15.1641	16.0633
0.8	0.00005	0.91463	14.782	16.1244
0.999	0.00005	0.91447	14.2971	16.1977
0	0.0001	0.89423	13.2408	12.2499
0.6	0.0001	0.89379	12.6854	12.3961
0.8	0.0001	0.89348	12.2607	12.4962
0.999	0.0001	0.89311	11.726	12.6104
0	0.00015	0.88038	12.1508	10.3061
0.6	0.00015	0.87958	11.5381	10.5404
0.8	0.00015	0.87903	11.0752	10.6868
0.999	0.00015	0.87841	10.4979	10.8437
0	0.0002	0.87909	11.5325	8.8917
0.6	0.0002	0.87843	10.8552	9.2956
0.8	0.0002	0.87763	10.3537	9.5055
0.999	0.0002	0.87733	9.7360	9.7115

$$f_{rms}(r) = Q^2(12\alpha r^4 - 9Mr) + \alpha r^5(4r - 15M) + Mr^2(6M - r) - 4Q^4 = 0. \tag{86}$$

The radii of ISCO and OSCO for different values of the parameters α and Q are presented in Fig. 25.

In order to show how the radii of the MSCOs of massive particles, the radius of the photon orbit, the radii of the horizons, and the static radius depend on the parameter α, we express α as a function of the radial coordinate r from Eqs. (86), (84), and (75).

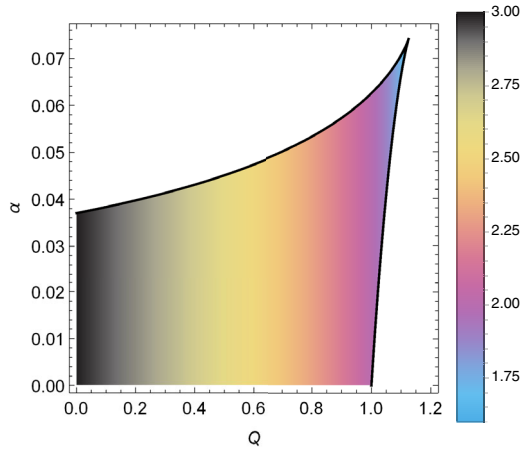

FIG. 24. Color map demonstrates the radii of photon orbits for different values of the parameters α and Q, for fixed $M = 1$. The radius of the photon orbit does not depend on α, but the parameter α defines the region where the existence of the black hole spacetime is allowed. Parameter Q changes from 0 to $Q_{\max}$, and parameter α takes values from 0 to $\alpha_{h(\max)}$ if $0 \leq Q < 1$, and $\alpha_{h(\min)} \leq Q < \alpha_{h(\max)}$ if $Q \geq 1$. The functions $\alpha_{h(\min)}$ and $\alpha_{h(\max)}$ are given by the conditions in Eqs. (77) and (76) for each value of parameter Q.

From Eq. (75), one can express the parameter α as a function of the radial coordinate r and Q in the following form:

$$\alpha_h(r) = \frac{r^2 - 2Mr + Q^2}{r^4}. \tag{87}$$

From Eq. (86), one can express the parameter α as a function of the radial coordinate r and Q in the following form:

$$\alpha_{ms}(r) = \frac{6M^2r^2 - 9MQ^2r - Mr^3 + 4Q^4}{r^4(-15Mr + 12Q^2 + 4r^2)}. \tag{88}$$

From Eq. (80), one can express the parameter α as a function of the radial coordinate r and Q in the following form:

$$\alpha_{rst}(r) = \frac{Mr - Q^2}{r^4}. \tag{89}$$

Figure 26 allows us to determine the existence of an event horizon, stable circular orbits, photon orbit, and static radius for two values of Q and certain values of α. If the choice of parameters allows the existence of these quantities, then it is possible to determine the corresponding radii from Fig. 26.

For each value of the parameter Q, there is a maximum value of the parameter $\alpha_{\max}(Q)$, which defines the region of stable circular orbits. Taking the derivative with respect to r from Eq. (88) for $\alpha_{ms}(r)$ and equating the resulting expression to 0, one can obtain the value of r_{crit} that determines the radius of a stable circular orbit for values of the parameter Q from 0 to $Q_{\max}$. By substituting the obtained value of r_{crit} for given Q into Eq. (88) for $\alpha_{ms}(r)$, we obtain the maximum value of the parameter $\alpha_{\max}(Q)$ for a stable circular orbit for the given value of Q. The thick red line in Fig. 20 shows the dependence of the maximum value for the parameter α on Q, and the shaded area under the thick red line in Fig. 20 determines the values of the parameters α and Q for which stable circular orbits exist.

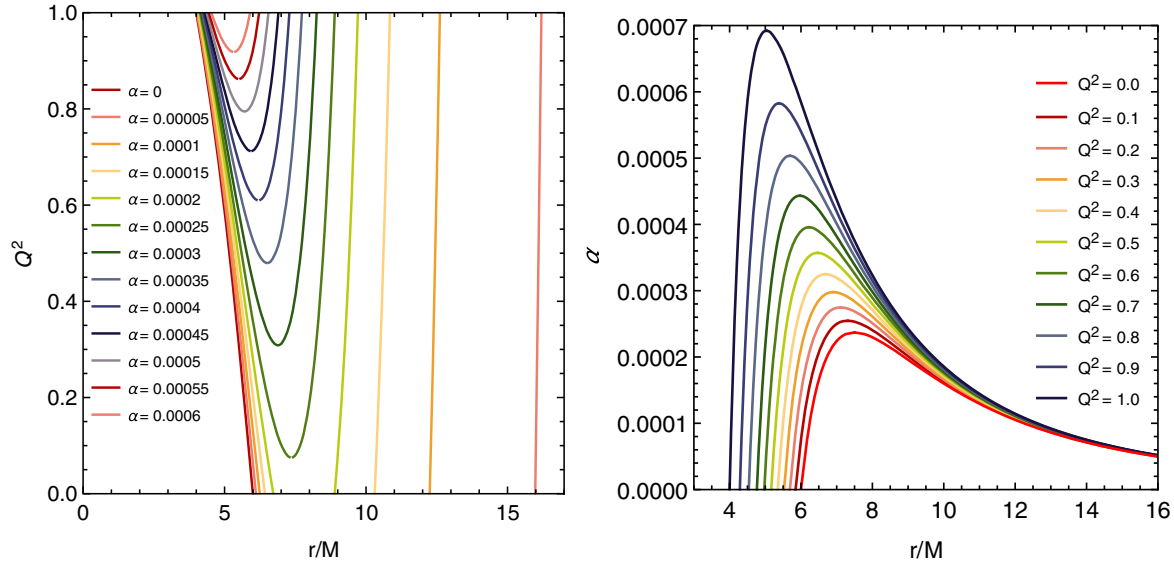

FIG. 25. In the left plot, the dependence of the radii of ISCO and OSCO for the whole range of Q^2 is shown; each graph is for different values of α, from $\alpha = 0$ to $\alpha = 0.0006$. In the right plot, the dependence of the radii of ISCO and OSCO for the whole range of α is shown; each graph corresponds to different values of Q^2, from $Q^2 = 0$ to $Q^2 = 1.0$.

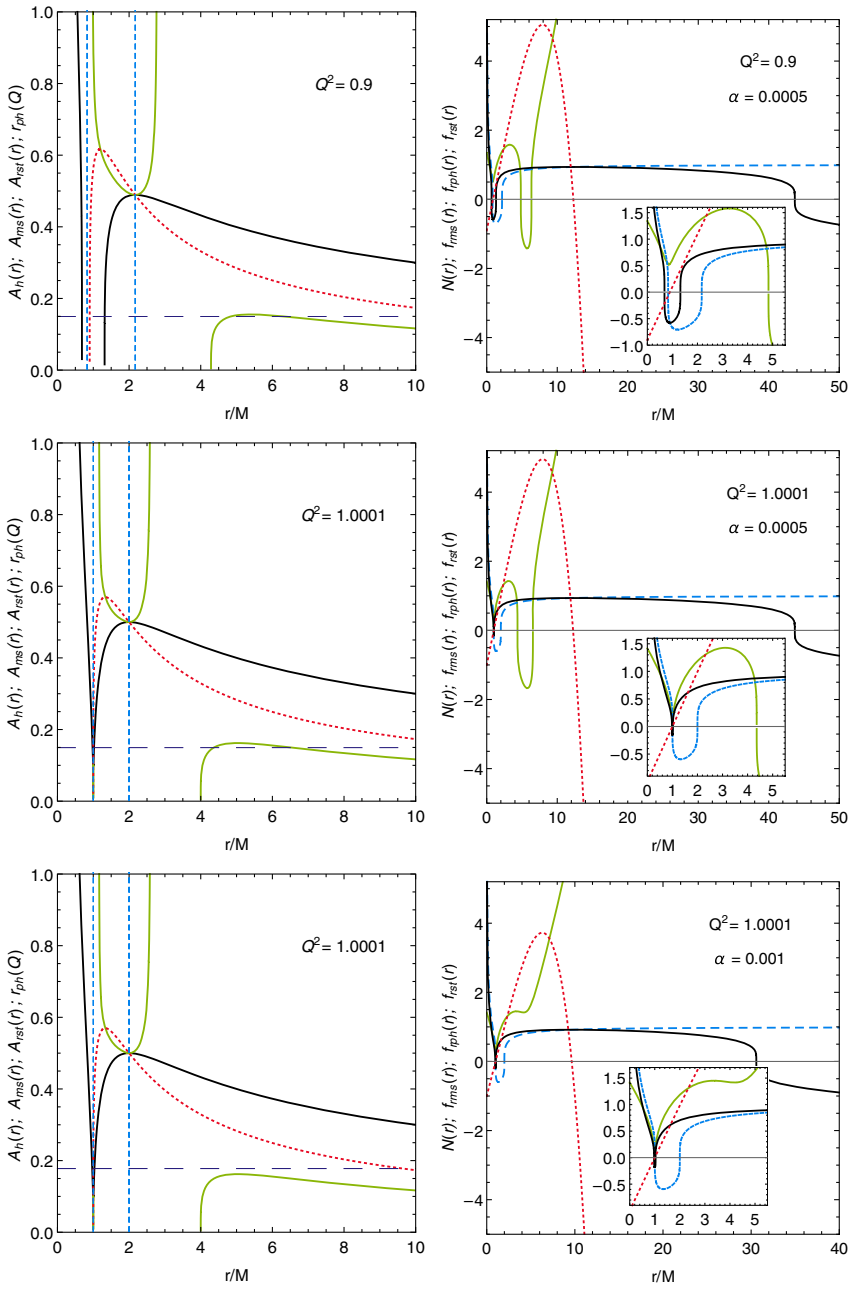

FIG. 26. Plots in the left column show the radial dependences of the functions $\alpha_h(r), \alpha_{rst}(r), \alpha_{ms}(r)$ and $r_{ph}(Q)$ [Eqs. (87), (89), (88), and (85) in the text; $r_{ph}(Q)$ does not depend on α in the case $w_q = -1$] for several values of the parameter Q with fixed $M = 1$. For better visualization, instead of the functions themselves in the plots, we show $A_h(r) = Sgn(\alpha_h(r))|\alpha_h(r)|^{1/4}$, $A_{rst}(r) = Sgn(\alpha_{rst}(r))|\alpha_{rst}(r)|^{1/4}$, and $A_{ms}(r) = Sgn(\alpha_{ms}(r))|\alpha_{ms}(r)|^{1/4}$. The thin black line is the graph of the function $A_h(r)$, which determines the positions of the event horizons. The blue dashed line is the graph of the function $r_{ph}(Q)$, which determines the position of the photon orbit. The thin green line is the graph of the function $A_{ms}(r)$, which determines the positions of the MSCOs. The red dotted line is the graph of the function $A_{rst}(r)$, which determines the position of the static radius. The gray dashed horizontal line represents the chosen value of the parameter $\alpha^{1/4}$; intersections with this line determine the positions of the horizons, photon circular orbit, MSCOs, and static radius. For the value of the parameter α represented by the gray dashed horizontal line, in the right column, the functions $N(r)$, $f_{rph}(r)$, $f_{rms}(r)$, and $f_{rst}(r)$ are shown; the zero values of these functions determine the radii of the corresponding quantities (event horizons, photon orbit, ISCO and OSCO, static radius). In the right column, for some values of the parameters α and Q, the following graphs are presented: The thin black line is the graph of the function $N(r)$ [Eq. (74)]; zero values of this function determine the positions of the horizons for the selected values of the parameter α. The blue dashed line is the graph of the function $f_{rph}(r)$ [Eq. (84)]; zero values of this function determine the position of the photon orbit for the selected values of the parameter α. The thin green line is the graph of the function $f_{rms}(r)$ [Eq. (86)]; zero values of this function determine the position of the ISCO for the selected values of the parameter α. The red dotted line is the graph of the function $f_{rst}(r)$ [Eq. (80)]; zero values of the function determine the position of the static radius for the selected values of the parameter α. Parameters α and Q take the values $\alpha = [0.0005, 0.001]$ and $Q = [0.9, 1.0001]$.

IV. OSCILLATIONS OF TEST PARTICLES NEAR MSCOs IN THE VICINITY OF A CHARGED KISELEV BLACK HOLE

In this section, we show how the fundamental frequencies of the test particles, performing epicyclic oscillatory motion along orbits slightly above the ISCO, depend on the parameters α and Q for the three different values of ω_q. Here we also give their radial profiles. We use the method based on the effective potential as discussed in Ref. [63]. The resulted frequencies are identical to those derived by the perturbation methods as shown in Ref. [68]. The derivation of the equations of the epicyclic frequencies is provided in the Appendix.

The radial epicyclic frequency reads

$$\nu_r = -\frac{1}{2\pi}\sqrt{\frac{N(r)^3}{2E^2}\frac{\partial^2 W_{\rm eff}(r,\theta)}{\partial r^2}}, \tag{90}$$

and the latitudinal epicyclic frequency ν_θ takes the following form:

$$\nu_\theta = -\frac{1}{2\pi}\sqrt{\frac{1}{2E^2}\frac{N(r)^2}{r^2}\frac{\partial^2 W_{\rm eff}(r,\theta)}{\partial \theta^2}}. \tag{91}$$

The azimuthal (so-called Keplerian) frequency of the test particle reads

$$\nu_\phi = \frac{\Omega_\phi}{2\pi} = \frac{1}{2\pi}\frac{L}{E}\frac{N(r)}{r^2}, \tag{92}$$

where $\Omega_\phi = d\phi/dt$ is the angular velocity of the test particle. In spherically symmetric spacetimes, $\nu_\theta = \nu_\phi$.

A. Oscillations of test particles near MSCOs of the charged Kiselev black hole with $\omega_q = -1/3$

The coinciding azimuthal and latitudinal frequency are equal to

$$\nu_\phi = \nu_\theta = \frac{1}{2\pi r^2}(Mr - Q^2)^{\frac{1}{2}}. \tag{93}$$

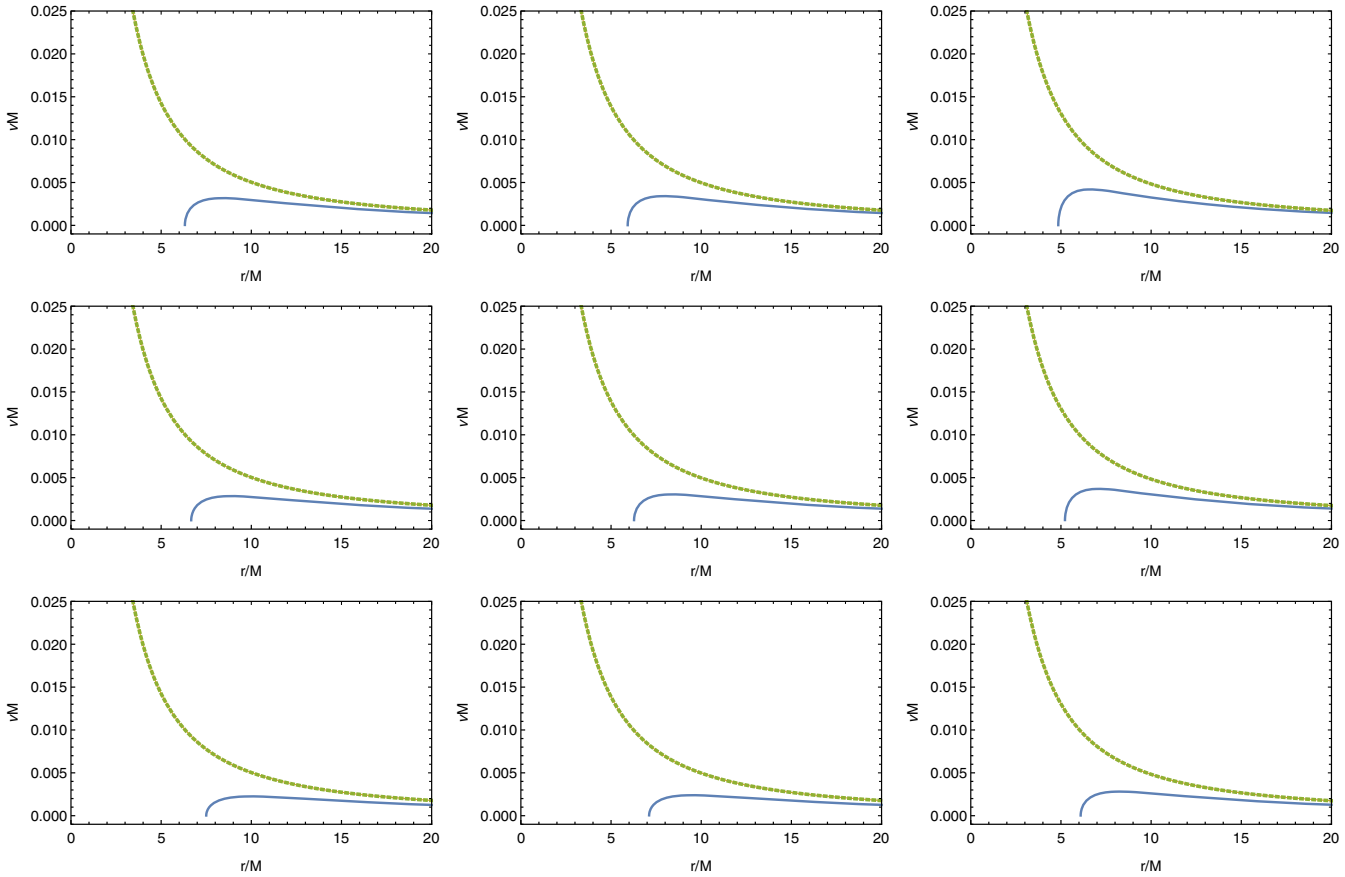

FIG. 27. Fundamental frequencies of a test particle for $\omega_q = -1/3$, and for the different values of parameters α and Q. $\alpha = 0.05, 0.1, 0.2$ in the first, second, and third rows, respectively; $Q = 0, 0.5, 0.9$ in the first, second, and third columns, respectively.

The radial epicyclic frequency is given by

$$\nu_r = \frac{1}{2\pi r^3}(Mr^2(r - r\alpha - 6M) + 9MQ^2r - 4Q^4)^{\frac{1}{2}}. \quad (94)$$

Figure 27 demonstrates the radial dependence of fundamental frequencies for different values of the parameters α and Q.

B. Oscillations of test particles near MSCOs of the charged Kiselev black hole with $\omega_q = -2/3$

The azimuthal and latitudinal frequencies coincide again in this case and take the following form:

$$\nu_\phi = \nu_\theta = \frac{\sqrt{2}}{4\pi r^2}(2Mr - 2Q^2 - \alpha r^3)^{\frac{1}{2}}. \quad (95)$$

Here, the radial epicyclic frequency is

$$\nu_r = \frac{\sqrt{2}}{4\pi r^3}(2Mr^2(r - 6M) - 8Q^4 - 3\alpha r^4(r - 4M) + \alpha^2 r^6 + Q^2(18Mr - 11\alpha r^3))^{\frac{1}{2}}. \quad (96)$$

Figure 28 represents the radial dependence of the fundamental frequency for different values of the parameters α and Q.

C. Oscillations of test particles near MSCOs of the charged Kiselev black hole with $\omega_q = -1$ (cosmological constant)

In this case, the azimuthal and latitudinal frequencies are

$$\nu_\phi = \nu_\theta = \frac{1}{2\pi r^2}(Mr - Q^2 - \alpha r^4)^{\frac{1}{2}}. \quad (97)$$

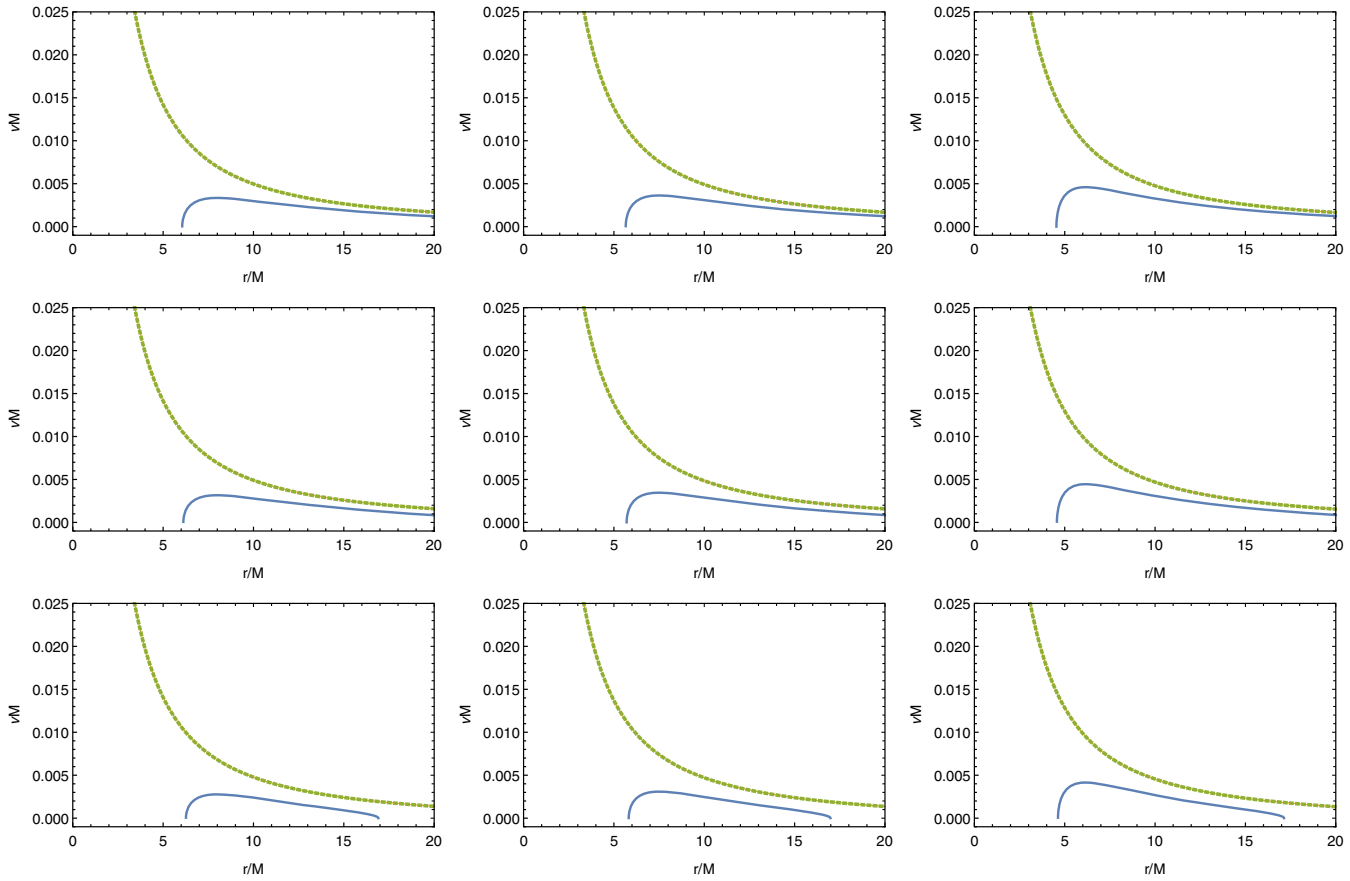

FIG. 28. Fundamental frequencies of a test particle for $\omega_q = -2/3$, and for the different values of parameters α and Q. $\alpha = 0.0005, 0.001, 0.002$ in the first, second, and third rows, respectively; $Q = 0, 0.5, 0.9$ in the first, second, and third columns, respectively.

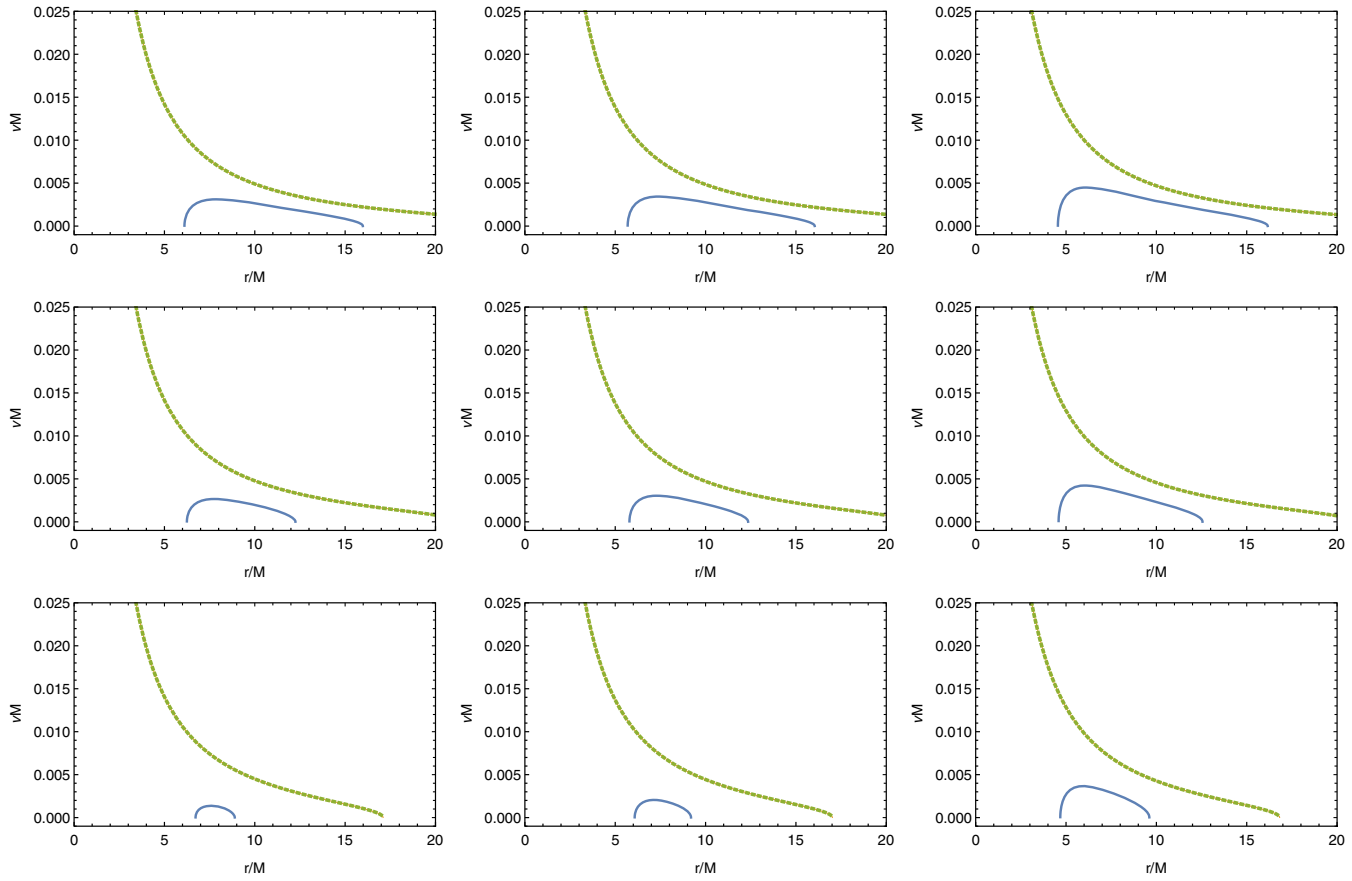

FIG. 29. Fundamental frequencies of a test particle for $\omega_q = -1$, and for the different values of the parameters α and Q. $\alpha = 0.00005, 0.0001, 0.0002$ in the first, second, and third rows, respectively; $Q = 0, 0.5, 0.9$ in the first, second, and third columns, respectively.

The radial epicyclic frequency takes the following form:

$$\nu_r = \frac{1}{2\pi r^3}(Mr^2(r-6M) - 4Q^4 + (15M-4r)\alpha r^5 + 3Q^2(3Mr - 4\alpha r^4))^{\frac{1}{2}}. \quad (98)$$

Figure 29 represents the radial dependence of fundamental frequency for the different values of the parameters α and Q.

V. APPLICATIONS TO REAL ASTROPHYSICAL SCENARIOS

In order to estimate the effects of quintessence fields on particle motion, we have considered a supermassive black hole $M = 10^6\ M_\odot$, and provide simple numerical estimation for the radial four-acceleration equation (38) (which is proportional to the radial force) of the test particle on different radii for three values of the parameter ω_q, in the cases of zero and nonzero charge parameter Q. We come to the conclusion that for the physically relevant value of the parameter α ($\alpha = 10^{-52}$ m^{-2} in the case of $\omega_q = -1$), and also for value of the parameter α ($\alpha = 10^{-28}$ m^{-1} in case of $\omega_q = -2/3$) and two values of the charge, $Q = 0$ and $Q = 10^6$ C, the effects of the considered spacetime with the repulsive constant α are not noticeable for the region near the black hole in comparison to the Schwarzschild spacetime, but far from the black hole, the effects of the considered spacetime become noticeable, and after a static radius where attraction and repulsion are balanced, repulsion becomes the dominant force. For the values of the parameter α ($\alpha = 10^{-26}$ m^{-2} in the case of $\omega_q = -1$, $\alpha = 10^{-14}$ m^{-1} in the case of $\omega_q = -2/3$), the effects of the considered spacetime are also noticeable near to the black hole, but the radius of the cosmological horizon which appears in considered spacetime is much smaller than the radius of the visible Universe. For the parameter $\omega_q = -1/3$, the difference between the acceleration of particle in Schwarzschild spacetime, and in the spacetime considered here, is noticeable for the value of the parameter $\alpha = 10^{-3}$ and is not noticeable for the value of $\alpha = 10^{-6}$. In the graphs in Fig. 30, we compare the acceleration of the test particle in the considered spacetime for the three different values of ω_q, for some representative values of

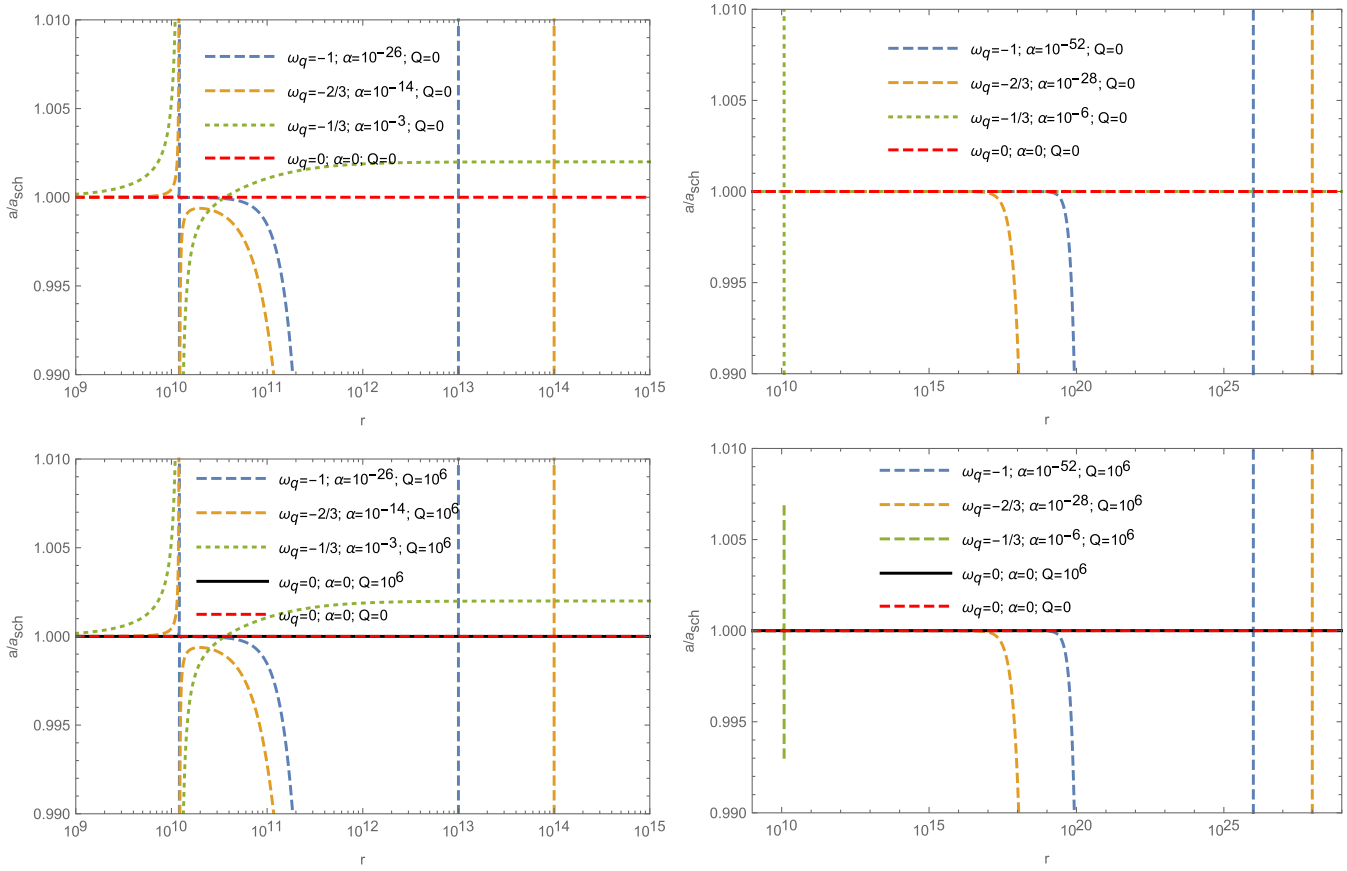

FIG. 30. The plots show a comparison of the acceleration acting on a particle located in the gravitational field of a Kiselev black hole with mass $M = 10^6\ M_\odot$ for three values of the parameter ω_q, with a Schwarzschild black hole in the case of zero charge Q (top two graphs), as well as with a Riessner-Nordstrom black hole for a charge $Q = 10^6$ C (lower two graphs). For nonzero values of the parameter α, the graphs diverge at the horizons.

α and Q, with the acceleration in the Schwarzschild spacetime. In the case of the charge $Q = 10^{26}$ C, the effects of the charge on the acceleration of the test particle also become noticeable and are presented in Fig. 31.

VI. SUMMARY

In this work, we have extensively investigated the MSCOs in the charged Kiselev black hole spacetime. We have taken into account three different values of the equations of state parameter ω_q, namely (i) $\omega_q = -1/3$, (ii) $\omega_q = -1$, and (iii) $\omega_q = -2/3$. For all three values of ω_q, we have obtained bounds on the values of the electric charge Q which allow the existence of a black hole and depend on the normalization factor α. These are represented in Figs. 1, 10, and 19 for the three values of parameter ω_q.

It is seen that the MSCOs exist for all possible values of the normalization factor α and the electric charge Q of the black hole, in all three cases for different values of the parameter ω_q.

Further, we have observed that the presence of the quintessence field pushes the ISCOs of the test particles outward, while the OSCOs contract. With decreasing values of the parameter α, ISCO in the charged Kiselev black hole spacetime approaches the ISCO for the pure Riessner-Nordstrom black hole, while OSCO pushes beyond the radius of the observable Universe. It is also observed that the radii of the ISCOs shrink due to the presence of the charge Q of the black hole, while those of the OSCOs get larger in the presence of the charge Q. This effect of charge Q on the radii of the MSCOs for the charged black hole with a quintessence term can be seen by comparing them with those obtained in the case of an uncharged black hole with the quintessence term, given in Ref. [53].

We have also studied the photon circular orbits and noticed that they expand in the presence of the quintessence field and shrink with an increase in the value of the charge Q of the black hole. Note that properties of the unstable photon circular orbit can also govern quasinormal modes of black hole perturbation fields [97,98].

Finally, we have studied epicyclic frequencies around charged Kiselev black holes and observed that they coincide in the azimuthal and longitudinal directions.

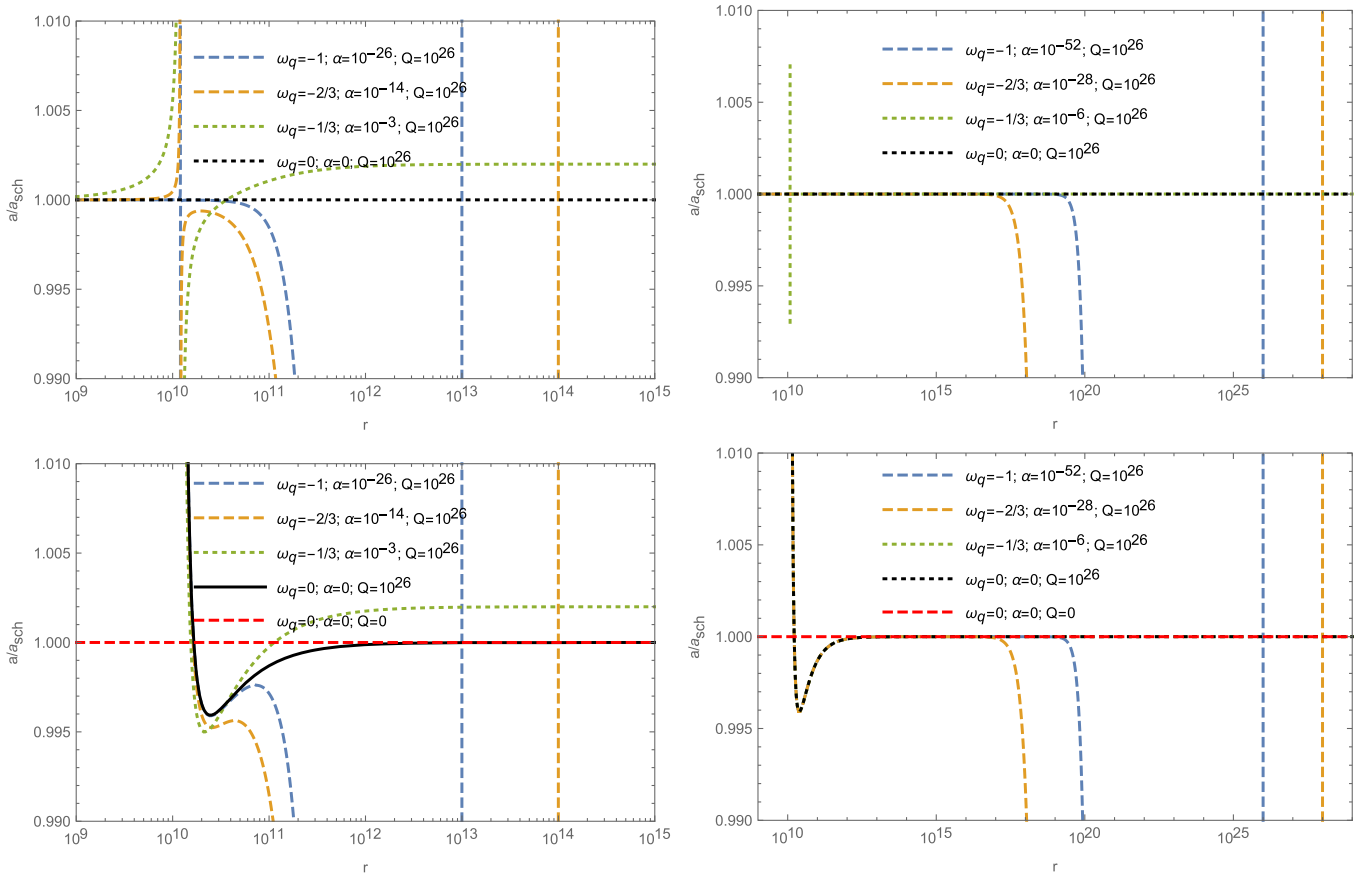

FIG. 31. The plots show a comparison of the acceleration acting on a particle located in the gravitational field of a Kiselev black hole with mass $M = 10^6\ M_\odot$ for three values of the parameter ω_q, with a Riessner-Nordstrom black hole (top two graphs), as well as with a Schwarzschild black hole (lower two graphs), with a charge $Q = 10^{26}$ C for both cases. For nonzero values of the parameter α, the graphs diverge at the horizons.

In addition, we have compared them with the frequencies for an uncharged black hole (when electric charge Q is equal to zero). With the increase of a black hole's electric charge Q, the ISCO becomes closer to the central object, and one can observe epicyclic frequencies closer to the central object, which makes the epicyclic frequencies larger. With increasing α, the ISCOs expand, and hence the epicyclic frequencies can be observed farther away from the central object. Thus, the presence of the quintessence field makes the epicyclic frequencies measured on the ISCOs smaller, as compared to the epicyclic frequencies in the vicinity of a Riessner-Nordstrom black hole without quintessence. With an increase in the charge Q of the black hole, the OSCOs stretch, and therefore the epicyclic frequencies can be smaller in comparison to the uncharged case of a black hole. It is also seen that the increasing values of α shrink the OSCOs, and therefore near OSCOs, the epicyclic frequencies can be higher due to the presence of the quintessence field. The obtained results can be applied to the real astrophysical scenario in black hole close environments to get possible constraints on the black hole's basic parameters and quintessence field.

ACKNOWLEDGMENTS

We acknowledge the institutional support of Silesian University in Opava. This research is supported by grants of the Ministry of Innovative Development of the Republic of Uzbekistan. Z. S. and D. O. acknowledge Grant No. 19-03950S of the Czech Science Foundation (GACR), and the internal student grant of the Silesian University in Opava, Grant No. SGS/12/2019. A. A. is supported by the PIFI fund of Chinese Academy of Sciences. We also acknowledge the anonymous referee for useful comments that helped to improve the text of the manuscript.

APPENDIX: DERIVATION OF EQUATIONS FOR FUNDAMENTAL FREQUENCIES

The procedure of finding equations for fundamental frequencies is quite standard—they can be obtained by direct perturbation of the geodetic equation as was done, for example, in Ref. [99]. In this appendix, we briefly review the algorithm presented in Ref. [73] for obtaining equations for fundamental frequencies where oscillations in the radial and vertical directions are considered separately.

The geodesic motion of the particle is governed by the Lagrangian

$$\mathcal{L} = \frac{1}{2} g_{\mu\nu} \dot{x}^\mu \dot{x}^\nu. \tag{A1}$$

We can notice that the metric that describes a charged Kisselev black hole does not depend explicitly on the coordinates t and ϕ. This means that there are constants of motion related to these coordinates:

$$p_t = \frac{\partial \mathcal{L}}{\partial \dot{t}} = g_{tt}\dot{t} = -E \Rightarrow \dot{t} = -\frac{E}{g_{tt}}, \tag{A2}$$

$$p_\phi = \frac{\partial \mathcal{L}}{\partial \dot{\phi}} = g_{\phi\phi}\dot{\phi} = L \Rightarrow \dot{\phi} = \frac{L}{g_{\phi\phi}}. \tag{A3}$$

We can find fundamental frequencies using an equation that describes the conservation of the rest mass, $g_{\mu\nu}\dot{x}^\mu \dot{x}^\nu = -1$. For spherically symmetric spacetime, it takes the form

$$g_{tt}(\dot{t})^2 + g_{rr}(\dot{r})^2 + g_{\theta\theta}(\dot{\theta})^2 + g_{\phi\phi}(\dot{\phi})^2 = -1. \tag{A4}$$

Now, we can apply to this equation $\dot{t}$ and $\dot{\phi}$ expressed using the constants of motion, and rearrange the equation in the following way:

$$g_{rr}(\dot{r})^2 + g_{\theta\theta}(\dot{\theta})^2 = -1 - \frac{E^2}{g_{tt}} - \frac{L^2}{g_{\phi\phi}}. \tag{A5}$$

The right-hand side of this equation can be denoted as $W_{\text{eff}}(r,\theta)$, some function which depends on r and θ, and in our notation for the interval of spherically symmetric static spacetime, it can be written as follows:

$$W_{\text{eff}}(r,\theta) = -1 + \frac{E^2}{N(r)} - \frac{L^2}{r^2 \sin^2\theta}. \tag{A6}$$

Now, we can consider small perturbations around circular orbits separately for the radial and vertical directions. For the radial direction, we assume $\dot{\theta} = 0$ and $g_{rr}(\dot{r})^2 = W_{\text{eff}}(r,\theta)$, and for the vertical direction, we assume $\dot{r} = 0$ and $g_{\theta\theta}(\dot{\theta})^2 = W_{\text{eff}}(r,\theta)$. Considering small displacements around the mean orbit δ_r and δ_θ—i.e., $r = r_0 + \delta_r$ and $\theta = \pi/2 + \delta_\theta$—and neglecting the terms of higher order $O(\delta_r^2)$ and $O(\delta_\theta^2)$, one can obtain equations for oscillating particles:

$$\frac{\mathrm{d}^2\delta_r}{\mathrm{d}t^2} + \Omega_r^2 \delta_r = 0, \qquad \frac{\mathrm{d}^2\delta_\theta}{\mathrm{d}t^2} + \Omega_\theta^2 \delta_\theta = 0, \tag{A7}$$

where Ω_r is related to the radial epicyclic frequency by $\nu_r = \Omega_r/2\pi$, and Ω_θ is related to the latitudinal frequency by $\nu_\theta = \Omega_\theta/2\pi$.

[1] D. Y. Chen, Q. Q. Jiang, and S. Z. Yang, Int. J. Theor. Phys. **46**, 3275 (2007).
[2] A. Abdujabbarov and B. Ahmedov, Phys. Rev. D **81**, 044022 (2010).
[3] V. Enolskii, B. Hartmann, V. Kagramanova, J. Kunz, C. Lammerzahl, and P. Sirimachan, Phys. Rev. D **84**, 084011 (2011).
[4] A. Abdujabbarov, B. Ahmedov, and A. Hakimov, Phys. Rev. D **83**, 044053 (2011).
[5] M. R. Setare and D. Momeni, Int. J. Theor. Phys. **50**, 106 (2011).
[6] Z. Stuchlík, M. Blaschke, and J. Schee, Phys. Rev. D **96**, 104050 (2017).
[7] M. Blaschke and Z. Stuchlík, Phys. Rev. D **94**, 086006 (2016).
[8] D. Pugliese, H. Quevedo, and R. Ruffini, Phys. Rev. D **83**, 024021 (2011).
[9] D. Pugliese, H. Quevedo, and R. Ruffini, Phys. Rev. D **83**, 104052 (2011).
[10] D. Pugliese, H. Quevedo, and R. Ruffini, Phys. Rev. D **84**, 044030 (2011).
[11] S. Fernando, Gen. Relativ. Gravit. **44**, 1857 (2012).
[12] I. Hussain, Mod. Phys. Lett. A **27**, 1250017 (2012).
[13] I. Hussain, Mod. Phys. Lett. A **27**, 1250068 (2012).
[14] I. Hussain, J. Phys. Conf. Ser. **354**, 012007 (2012).
[15] J. Sadeghi and B. Pourhassan, Eur. Phys. J. C **72**, 1984 (2012).
[16] D. Pugliese, H. Quevedo, and R. Ruffini, Phys. Rev. D **88**, 024042 (2013).
[17] V. Frolov and D. Stojkovic, Phys. Rev. D **68**, 064011 (2003).
[18] A. M. Al Zahrani, V. P. Frolov, and A. A. Shoom, Phys. Rev. D **87**, 084043 (2013).
[19] A. A. Abdujabbarov, B. J. Ahmedov, and N. B. Jurayeva, Phys. Rev. D **87**, 064042 (2013).
[20] E. Li and Y. Zhang, Astrophys. Space Sci. **350**, 361 (2014).
[21] S. Hussain, I. Hussain, and M. Jamil, Eur. Phys. J. C **74**, 3210 (2014).
[22] L. Rezzolla and A. Zhidenko, Phys. Rev. D **90**, 084009 (2014).
[23] I. Hussain, B. Majeed, and M. Jamil, Int. J. Theor. Phys. **54**, 1567 (2015).

[24] A. Garcia, E. Hackmann, J. Kunz, C. Lämmerzahl, and A. Macias, J. Math. Phys. (N.Y.) **56**, 032501 (2015).
[25] R. Uniyal, N. C. Devi, H. Nandan, and K. D. Purohit, Gen. Relativ. Gravit. **47**, 16 (2015).
[26] T. Ono, T. Suzuki, N. Fushimi, K. Yamada, and H. Asda, Europhys. Lett. **111**, 30008 (2015).
[27] M. Batool and I. Hussain, Int. J. Mod. Phys. D **26**, 1741005 (2017).
[28] G. Mustafa and I. Hussain, Eur. Phys. J. C **81**, 419 (2021).
[29] A. Tursunov, Z. Stuchlík, M. Kološ, N. Dadhich, and B. Ahmedov, Astrophys. J. **895**, 14 (2020).
[30] P. J. Peebles and B. Ratra, Rev. Mod. Phys. **75**, 559 (2003).
[31] B. Ratra and P. J. E. Peebles, Phys. Rev. D **37**, 3406 (1988).
[32] Z. Stuchlík, Bull. Astron. Inst. Czechosl. **34**, 129 (1983).
[33] Z. Stuchlík, Bull. Astron. Inst. Czechosl. **35**, 205 (1984).
[34] Z. Stuchlík and S. Hledík, Phys. Rev. D **60**, 044006 (1999).
[35] Z. Stuchlík and S. Hledík, Acta Phys. Slovaca **52**, 363 (2002).
[36] P. Slany and Z. Stuchlík, Classical Quantum Gravity **22**, 3623 (2005).
[37] Z. Stuchlík, Mod. Phys. Lett. A **20**, 561 (2005).
[38] Z. Stuchlík and J. Kovář, Int. J. Mod. Phys. D **17**, 2089 (2008).
[39] Z. Stuchlík, P. Slany, and J. Kovář, Classical Quantum Gravity **26**, 215013 (2009).
[40] Z. Stuchlík and J. Schee, J. Cosmol. Astropart. Phys. 09 (2011) 018.
[41] Z. Stuchlík, S. Hledík, and J. Novotny, Phys. Rev. D **94**, 103513 (2016).
[42] B. Toshmatov, Z. Stuchlík, and B. Ahmedov, Eur. Phys. J. Plus **132**, 98 (2017).
[43] Z. Stuchlík, D. Charbulák, and J. Schee, Eur. Phys. J. C **78**, 180 (2018).
[44] Z. Stuchlík, M. Kološ, J. Kovář, P. Slany, and A. Tursunov, Universe **6**, 26 (2020).
[45] V. V. Kiselev, Classical Quantum Gravity **20**, 1187 (2003).
[46] S. G. Ghosh, Eur. Phys. J. C **76**, 222 (2016).
[47] S. Shaymatov, B. Ahmedov, Z. Stuchlík, and A. Abdujabbarov, Int. J. Mod. Phys. D **27**, 1850088 (2018).
[48] C. A. Benavides-Gallego, A. Abdujabbarov, and C. Bambi, Phys. Rev. D **101**, 044038 (2020).
[49] H. Chakrabarty, A. Abdujabbarov, and C. Bambi, Eur. Phys. J. C **79**, 179 (2019).
[50] M. Visser, Classical Quantum Gravity **37**, 045001 (2020).
[51] W. Miranda, S. Carneiro, and C. Pigozzo, J. Cosmol. Astropart. Phys. 07 (2014) 043.
[52] I. Zlatev, L. M. Wang, and P. J. Steinhardt, Phys. Rev. Lett. **82**, 896 (1999).
[53] I. Hussain and S. Ali, Gen. Relativ. Gravit. **47**, 34 (2015).
[54] A. Younas, M. Jamil, S. Bahamonde, and S. Hussain, Phys. Rev. D **92**, 084042 (2015).
[55] M. Azreg-Aïnou, M. Jamil, and S. Bahamonde, Eur. Phys. J. C **77**, 414 (2017).
[56] B. Majeed, M. Jamil, and P. Pradhan, Adv. High Energy Phys. **2015**, 124910 (2015).
[57] M. Azreg-Aïnou, Eur. Phys. J. C **75**, 34 (2015).
[58] I. Hussain and S. Ali, Eur. Phys. J. Plus **131**, 275 (2016).
[59] S. M. J. Riaz, J. Astrophys. Astron. **39**, 64 (2018).
[60] L. Rezzolla, S'i. Yoshida, T. J. Maccarone, and O. Zanotti, Mon. Not. R. Astron. Soc. **344**, L37 (2003).
[61] G. Török, A. Kotrlová, E. Šrámková, and Z. Stuchlík, Astron. Astrophys. **531**, A59 (2011).
[62] Z. Stuchlík, A. Kotrlová, and G. Török, Astron. Astrophys. **525**, A82 (2011).
[63] Z. Stuchlík, A. Kotrlová, and G. Török, Astron. Astrophys. **552**, A10 (2013).
[64] L. Rezzolla and O. Zanotti, *Relativistic Hydrodynamics* (Oxford University Press, New York, 2013), ISBN-10: 0198528906; ISBN-13: 978-0198528906.
[65] S. Kato, Publ. Astron. Soc. Jpn. **60**, 111 (2008).
[66] M. A. Abramowicz, M. Jaroszynski, S. Kato, J. P. Lasota, A. Rozanska, and A. Sadowski, Astron. Astrophys. **521**, A15 (2010).
[67] O. Zanotti, L. Rezzolla, and J. A. Font, Mon. Not. R. Astron. Soc. **341**, 832 (2003).
[68] A. Tursunov, Z. Stuchlík, and M. Kološ, Phys. Rev. D **93**, 084012 (2016).
[69] M. Kološ, Z. Stuchlík, and A. Tursunov, Classical Quantum Gravity **32**, 165009 (2015).
[70] Z. Stuchlík and M. Kološ, Eur. Phys. J. C **76**, 32 (2016).
[71] M. Kološ, A. Tursunov, and Z. Stuchlík, Eur. Phys. J. C **77**, 860 (2017).
[72] M. Kološ, A. Tursunov, and Z. Stuchlík, Phys. Rev. D **103**, 024021 (2021).
[73] C. Bambi, *Black Holes: A Laboratory for Testing Strong Gravity* (Springer, Singapore, 2017), ISBN 978-981-10-4523-3, https://doi.org/10.1007/978-981-10-4524-0.
[74] V. V. Kiselev, arXiv:gr-qc/0303031.
[75] N. Varghese and V. C. Kuriakose, Gen. Relativ. Gravit. **41**, 1249 (2009).
[76] S. Fernando, Mod. Phys. Lett. A **28**, 1350189 (2013).
[77] S. Fernando, Gen. Relativ. Gravit. **45**, 2053 (2013).
[78] M. Azreg-Aïnou and M. E. Rodrigues, J. High Energy Phys. 09 (2013) 146.
[79] S. Fernando, S. Meadows, and K. Reis, Int. J. Theor. Phys. **54**, 3634 (2015).
[80] K. Ghaderi and B. Malakolkalami, Nucl. Phys. **B903**, 10 (2016).
[81] M. S. Ma, R. Zhao, and Y. Q. Ma, Gen. Relativ. Gravit. **49**, 79 (2017).
[82] H. Ghaffarnejad, E. Yaraie, and M. Farsam, Int. J. Theor. Phys. **57**, 1671 (2018).
[83] W. Hong, B. Mu, and J. Tao, Nucl. Phys. **B949**, 114826 (2019).
[84] A. S. M. Moinuddin and M. Hossain Ali, Mod. Phys. Lett. A **34**, 1950211 (2019).
[85] V. K. Shchigolev and D. N. Bezbatko, Gen. Relativ. Gravit. **51**, 34 (2019).
[86] P. Boonserm, T. Ngampitipan, A. Simpson, and Matt Visser, Phys. Rev. D **101**, 024022 (2020).
[87] H. Ghaffarnejad, M. Farsam, and E. Yaraie, Adv. High Energy Phys. **2020**, 9529356 (2020).
[88] E. Poisson, *A Relativist's Toolkit: The Mathematics of Black-Hole Mechanics* (Cambridge University Press, Cambridge, England, 2007), ISBN-10: 0521537800, ISBN-13: 978-0521537803.
[89] B. P. Dolan, Classical Quantum Gravity **36**, 077001 (2019).
[90] A. Vikman, Phys. Rev. D **71**, 023515 (2005).
[91] D. Spergel and Ue-Li Pen, Astrophys. J. **491**, L67 (1997).

[92] S. Kumar, A. Nutiyal, and A. A. Sen, Eur. Phys. J. C **73**, 2562 (2013).
[93] E. J. Copeland, M. Sami, and S. Tsujikawa, Int. J. Mod. Phys. D **15**, 1753 (2006).
[94] L. G. Collodel, B. Kleihaus, and J. Kunz, Phys. Rev. Lett. **120**, 201103 (2018).
[95] Z. Stuchlík and P. Slany, Phys. Rev. D **69**, 064001 (2004).
[96] J. Schee and Z. Stuchlík, Eur. Phys. J. C **76**, 643 (2016).
[97] E. Berti, V. Cardoso, and A. O. Starinets, Classical Quantum Gravity **26**, 163001 (2009).
[98] R. A. Konoplya and Z. Stuchlík, Phys. Lett. B **771**, 597 (2017).
[99] A. N. Aliev and D. V. Gal'tsov, Sov. Phys. Usp. **32**, 75 (1989).